




## Seismic Hazard Assessment and Its Uncertainty for the Central Part of Northern Algeria

M. HAMDACHE,<sup>1</sup>  J. A. PELÁEZ,<sup>2</sup> J. HENARES,<sup>3</sup> and R. SAWIRES<sup>4</sup>

**Abstract**—This study presents a probabilistic seismic hazard assessment for the central part of northern Algeria using two complementary seismic models: a fault-based model and a gridded seismicity model. Two ground-motion attenuation equations were chosen using the Pacific Earthquake Engineering Research Center Next-Generation models, as well as local and regional ones. The ranking method was used to assess their ability to gather accurate data. To account for epistemic uncertainty in both components of the assessment, the seismic hazard was computed using a logic tree approach. Expert judgment and data testing were used to evaluate the weights assigned to individual ground-motion prediction equations. The seismic hazard maps depicted the obtained results in terms of spectral accelerations at oscillation periods of 0.0, 0.2, and 1.0 s, with 10% and 5% probabilities of exceedance in 50 years, and for soil types B, B/C, C, and C/D, as defined by the National Earthquake Hazards Reduction Program. From the analysis, the uncertainty is expressed as both a 95% confidence band and the coefficient of variation (COV). Annual frequencies of exceedance and hazard curves were estimated for the selected cities, as well as uniform hazard spectra for the previously quoted probabilities of exceedance and the soil types considered. Peak ground acceleration values of  $0.44 \pm 0.17$  g and  $0.38 \pm 0.06$  g were reported for the B/C soil type in the cities of Algiers and Blida, respectively, for a return period of 475 years. Seismic maps for the selected return periods depicting the classification of the estimated values are also displayed in terms of very high, high, medium, low and very low degrees of reliability. Furthermore, a seismic hazard disaggregation analysis in terms of magnitude, distance, and azimuth was carried out. The primary goal of such analyses is to determine the relative contribution of different seismic foci and sources to seismic hazard at specific locations. Thus, for each studied city, for the considered return periods and for the soil type B/C, the so-called control or modal earthquake was estimated. At Algiers, events with magnitudes Mw 5.0–5.5 and distances of less than 10 km contribute the

most to the mean seismic hazard over a 475-year period. However, for the same return period, those events with Mw 7.0–7.5 and located between 10 and 20 km away contribute the most to the seismic hazard at Tipaza.

**Keywords:** Fault-based model, gridded seismicity model, seismic hazard, uniform hazard spectra, disaggregation, control earthquake, Algeria.

### 1. Introduction

Several damaging earthquakes have occurred in the central part of northern Algeria during recent times, indicating a high level of seismic activity (Hamdache et al., 2010). The May 21, 2003 (Mw 6.9) Zemmouri earthquake, which occurred about 50 km northeast of Algiers, was among the most significant. The earthquake of August 1, 2014 (Mw 5.5) hit the region of Algiers, with the surrounding areas shaken by this low- to moderate-magnitude earthquake. Regarding this seismic activity, the interest of the scientific community in the mitigation of destructive earthquakes and related seismic risk assessment investigations of urban areas in northern Algeria is steadily growing. As a result, various studies have been conducted in the past to assess the seismic hazard in major cities in the central part of northern Algeria. Among these studies are Benouar (1996) and Gherboudj et al. (2014) for Algiers, and Hamdache et al. (2012) for the most important cities in northern Algeria. The issue of urban planning, according to Mandal et al. (2013), is to estimate the ground-motion effects related to various sources and site characteristics with an acceptable level of confidence, not only for a single site, but also for all places with an acceptable level of reliability.

**Supplementary Information** The online version contains supplementary material available at <https://doi.org/10.1007/s00024-022-03066-0>.

<sup>1</sup> Seismological Division, CRAAG, B.P 63, 16006 Algiers, Algeria. E-mail: m\_hamdache@hotmail.com

<sup>2</sup> Department of Physics, University of Jaén, 23071 Jaén, Spain. E-mail: japelaez@ujaen.es

<sup>3</sup> International University of La Rioja, 26006 Logroño, Spain. E-mail: jesus.henares@unir.net

<sup>4</sup> Department of Geology, Faculty of Science, Assiut University, Assiut 71516, Egypt. E-mail: rashed.sawires@aun.edu.eg

The probabilistic seismic hazard assessment (PSHA) method was developed in the 1960s (Cornell, 1968) and is largely considered the state-of-the-art for seismic hazard evaluation in most regional, national, and international seismic regulations all over the world. Active fault-source identification and presentation is becoming more common in probabilistic seismic hazard evaluations, and this practice is growing in acceptance (e.g., Pace et al., 2016; Visini et al., 2020). As a result, the current study focuses on estimating seismic hazard in the central part of northern Algeria, which lies between  $1.5^\circ$  and  $4.0^\circ$  E and  $34.5^\circ$  to  $37.5^\circ$  N, using a fault-based source model and a gridded seismicity model. As well as the assessment of uncertainties affecting estimated values, which is becoming increasingly desirable.

A site-specific seismic hazard assessment was carried out for the main selected cities, taking into account the average shear wave velocity for the upper 30 m of the soil,  $V_S(30)$ , according to Shumway et al. (2018) and following the National Earthquake Hazards Reduction Program (NEHRP) classification (BSSC, 2003). Peak ground acceleration (PGA) and spectral acceleration (SA) values for oscillation periods of 0.2 and 1.0 s, estimated at 5% and 10% probability of exceedance in 50 years, and for soil conditions with  $V_S(30)$  equal to 760 m/s are represented on computed seismic hazard maps. Hazard curves as well as the uniform hazard spectra (UHS) for selected cities were also assessed for the previously stated return periods. The computed UHS, as well as the seismic hazard values, have been calculated for the NEHRP B, B/C, C, and C/D site classes, corresponding to  $V_S(30)$  values of 1150, 760, 537 and 360 m/s, respectively (Shumway et al., 2018). The soil classification proposed in the Algerian building code (RPA99, 2003) is slightly different. Four site classes are proposed and denoted as S1, S2, S3 and S4, with corresponding shear wave velocity ( $V_S$ ) range given by  $\geq 800$ , 400–800, 200–400, and 100–200 m/s, respectively. For instance, according to RPA99 (2003), site class S1 is for rock soil ( $V_S \geq 800$  m/s), and site class S2 is defined as deposits of very dense sand and gravel and/or over

consolidated clay 10 to 20 m thick, with  $V_S \geq 400$  m/s from 10 m depth. Similarly, the S3 site class is defined as thick deposits of moderately dense sands and gravels or moderately stiff clay with  $V_S \geq 200$  m/s from a depth of 10 m, and the S4 site class is defined as sand deposits with or without the presence of soft clay layers with  $V_S < 200$  m/s in the first 20 m; soft to moderately stiff clay deposits with  $V_S < 200$  m/s in the first 20 m. As can be seen, the proposed classification does not refer explicitly to the  $V_S(30)$  as the average shear wave velocity for the upper 30 m of the soil, making it inappropriate for use in the recent ground-motion prediction equations (GMPEs). According to Shumway et al. (2018), they must include a term for  $V_S(30)$  or be accompanied by other relationships, such as the amplification values that transfer their equations from a  $V_S(30)$  of 760 m/s to soil conditions. The values proposed by Shumway et al. (2018), adopted in the current study and used for the 2014 National Seismic Hazard Model (Petersen et al., 2015), are considered to be more consistent with building codes, which require the  $V_S(30)$  for site class centers as well as site class boundaries.

The obtained results are also expressed in terms of an overall 95% confidence band and an overall coefficient of variation (COV) for both return times and soil type B/C, based on the uncertainty analysis. Seismic maps depicting the classification of estimated values for the selected return periods are displayed in terms of very high, high, medium, low, and very low degrees of reliability for the selected return periods. The UHS and their standard deviation curves, as well as the seismic hazard curves and their 95% confidence limits, are displayed for each studied city and for the selected return periods. In addition, the contribution of different earthquake scenarios of magnitude–distance combinations ( $M, D$ ) to seismic hazard values at specific places is evaluated. The so-called control earthquake (Berneuter, 1992) or modal earthquake is derived and analyzed using a disaggregation analysis (Chapman, 1995). The seismic hazard also is disaggregated for the considered sites in terms of longitude and latitude (e.g., azimuth) to

quantify the contribution of the grid cells covering the study area.

## 2. Earthquake Catalog, Seismicity and Seismotectonic Context

The studied area, situated in the central part of northern Algeria, is geographically located in the Tell Atlas (see Fig. 1). This important geological structure

is the result of the collision triggered by the opening of the Algero-Provençal Basin within the Nubian Plate during the Early Miocene. It is likely also combined with a northward-dipping subduction process of the Nubian Plate (Peláez et al., 2018a, b). The current tectonic features are mainly presented as NE-SW to E-W on-shore and offshore folds and thrust faults (e.g., Déverchère et al., 2005; Morel & Meghraoui, 1996).

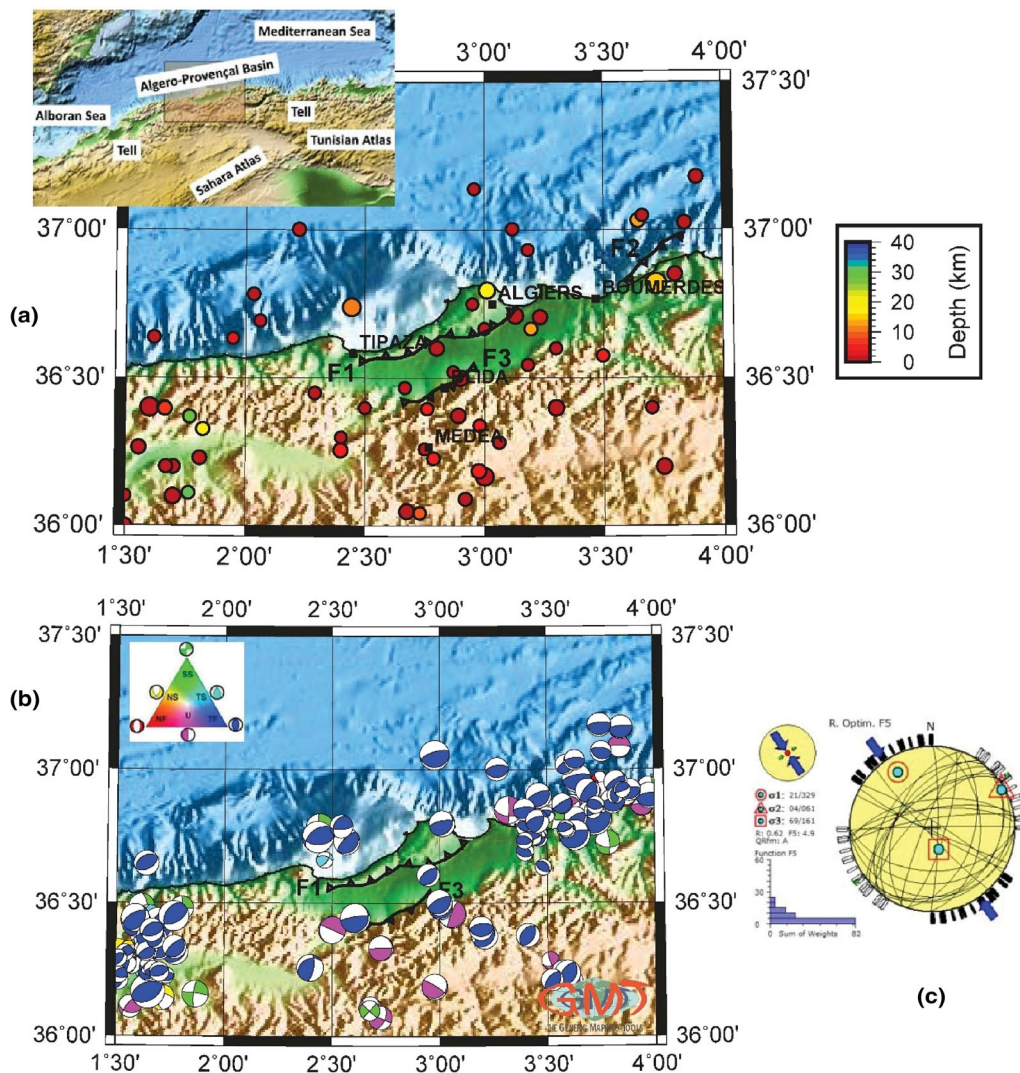


Figure 1

**a** Seismicity ( $M_w \geq 4.0$  from 1950) and **b** computed focal mechanism solutions ( $M_w \geq 3.0$ ) in the study area. **c** Lower-hemisphere equal area stereoplots (Peláez et al., 2018a), including associated slip lines, depicting the stress regime in the region. F1: Sahel Fault. F2: Zemmouri Fault. F3: Blida Fault

This region has experienced several damaging earthquakes in the past. Some examples are the January 03, 1365, and May 05, 1716 earthquakes, both felt with intensity X (European Macroseismic Scale, EMS-98) (Harbi et al., 2007). Another historical event is the earthquake that occurred on March 02, 1825, with a felt intensity of X-XI on the Modified Mercalli Intensity (MMI) scale. The most recent damaging earthquake that occurred in the studied region was the May 21, 2003 (Mw 6.9) event (Hamdache et al., 2010; Peláez et al., 2006b). Its epicenter was located in the eastern part of the Mitidja Basin. This basin is an E-W elongated coastal intermountain Quaternary Basin affected by an N-S to NNW-SSE-trending shortening (e.g., Maouche et al., 2011; Meghraoui & Doumaz, 1996). From the north, this basin is bounded by the Sahel Ridge, which runs along the Mediterranean coast and links the Chenoua to the Algiers-Bouzareah Massifs. A 60–70 km-long, NW-dipping blind thrust fault delimits this structure from the northern side (e.g., Meghraoui, 1991). However, from the south, the ENE-WSW-trending Blida fault system delimits the Mitidja Basin. This en echelon reverse fault system is located at the foot of the Blidean Atlas Mountains, showing Mesozoic to Cenozoic formations over thrusting the Neogene and Quaternary layers (Yelles et al., 2009) (Fig. 1b).

As previously stated, the Sahel anticline extends along the northern edge of the Mitidja Basin, hiding approximately 60–70 km of NW dipping thrust fault, the westernmost portion of which, according to Meghraoui (1991), was reactivated during the 1989 Tipaza earthquake (Mw 5.9). Belabbès et al. (2009) argue that due to the InSAR investigation and modeling of the 2003 Zemmouri earthquake rupture, because the two edges of the basin have been reactivated, during the 1989 Tipaza earthquake and 2003 Zemmouri earthquake, the central sections of either the Sahel anticline or the Blida thrust fault system must accommodate shortening movements. They explained that these structures could contribute to the seismic hazard assessment.

The earthquake data file compiled for northern Algeria by Hamdache et al. (2010) and updated through December 2018 is used in the current study. An updated Poissonian earthquake data file is an

essential component in conducting a valid PSHA study since it is the first step in developing and describing a reliable and representative seismic source model. The initial earthquake data file was assembled from a wide range of original data sources. The final result is a unified earthquake data file in terms of magnitude, spatial extent of 32° and 38° latitudes, 3°W and 10°E longitudes, and a time span of AD 856 to June 2008, which Hamdache et al. (2010) compiled by analyzing several published papers, bulletins, and data sources. It is worth noting that several fitting relationships between the reported magnitudes, maximum intensities, and moment magnitude were employed during the preparation of this catalog, in order to carry out the magnitude homogenization in terms of the moment magnitude scale ( $M_w$ ). In the case of the reported size of the event was the maximum intensity, the equivalent magnitude was computed from the Mezcua (2002) relationship.

$$M_w = 0.96 + 0.6 I_{\max}. \quad (1)$$

In this last case, and for offshore locations, epicentral intensity was calculated using the maximum intensity onshore and the intensity attenuation relationship developed by López Casado et al (2000). Whereas, for earthquakes with reported  $M_s$  or  $m_b$  magnitude, the relationships by Johnston (1996) were used to calculate the equivalent seismic moment, and then the magnitude  $M_w$  was derived using the relationship by Kanamori (1977)

$$\log M_0 = 24.66 - 1.883 M_s + 0.192 M_s^2; \quad (2)$$

$$(3.5 < M_s < 7.5),$$

$$\log M_0 = 18.28 - 0.679 m_b + 0.077 m_b^2; \quad (3)$$

$$(3.5 < m_b < 6.5).$$

Finally, the relationship by Rueda and Mezcua, (2002) was used to convert the magnitude  $m_{bLg}$  to the magnitude  $M_w$

$$M_w = 0.311 + 0.637 m_{bLg} + 0.061 m_{bLg}^2; \quad (4)$$

$$(1.7 < m_{bLg} < 5.7).$$

It is worth noting that, according to Bakun (1984) and Heaton et al. (1986), the equivalent moment magnitude for earthquakes with a reported  $M_L$



magnitude computed from the duration of the record is roughly identical to this value.

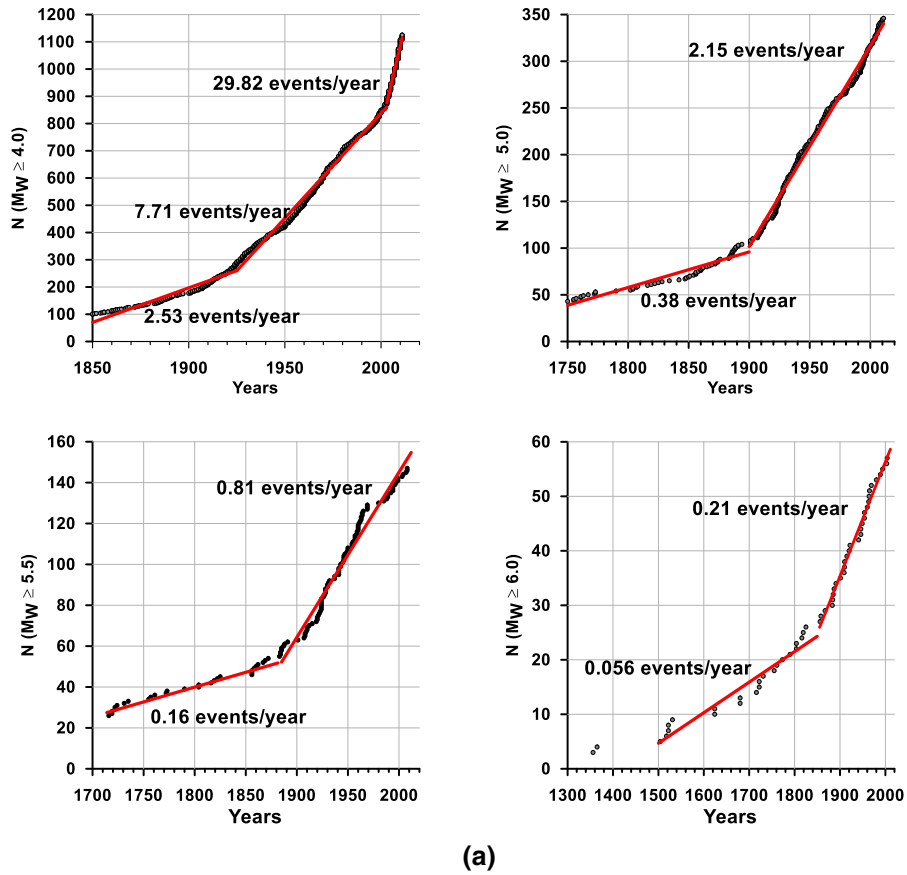
Figure 1a depicts the spatial distribution of seismicity for earthquakes with magnitudes greater than  $M_w$  4.0. Figure 1b shows the computed focal mechanism distribution of earthquakes in the study area using the focal mechanism data file compiled by Peláez et al. (2018a, 2018b). Furthermore, the stress regime pattern for those delineated sources was computed using the available focal mechanism solutions from the Delvaux and Sperner (2003) inversion method using the Win-Tensor<sup>TM</sup> software. Figure 1c depicts the lower-hemisphere equal-area stereo plots of the focal planes selected for the study area. The dominating stress field in the examined region, according to Peláez et al. (2018a, b), is a NNW-SSE trending pure compressional regime.

The next step was to remove any dependent (non-Poissonian) earthquakes (foreshocks, aftershocks, and seismic swarms). The procedure by Gardner and Knopoff (1974) was used in accordance with the specific temporal and spatial windows introduced by Hamdache et al. (2010). The statistical approach to completeness assessment began with the work by Stepp (1972). Several methods are frequently used to analyze the completeness of a catalog, all of which are based on the assumption that earthquakes with magnitudes greater than a given value exhibit Poissonian behavior, implying that the earthquake file, or catalog, should be declustered before performing any completeness analysis. A comprehensive review of existing methods is beyond the scope of this study. Some examples are given, including those by Albarello et al. (2001) and Mignan and Woessner (2012). In the current study, as in Peláez et al. (2003) and Hamdache et al. (2010), the approach developed by EPRI (1986) is used to derive the threshold magnitude of the earthquake data file. This procedure is similar to the approach used by Salazar et al. (2013) based on the Tinti and Mulargia (1985) method. It appears suitable to apply this visual approach to the current study, suggesting that earthquakes above a given magnitude are complete and Poissonian if the cumulative annual number above the given magnitude is approximately linear.

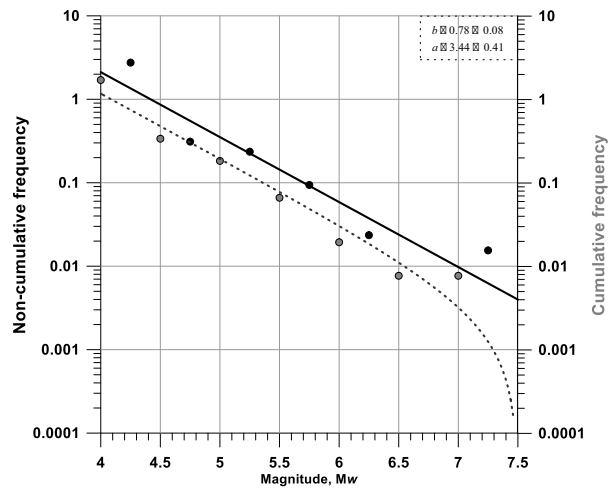
Thus, the completeness catalog and the Poissonian character can be inferred from Fig. 2a, depicting

the cumulative number of earthquakes above magnitude  $M_w$  4.0, 5.0, 5.5 and 6.0. It appears that magnitudes  $M_w$  4.0 and 5.0 are likely complete and Poissonian since 1925 and 1900 for the whole data file, with rates of 7.71 and 2.15 events/year, respectively, and that magnitudes  $M_w$  5.5 and 6.0 are likely complete and Poissonian since 1885 and 1855 with rates of 0.81 and 0.21 events/year, respectively. In recent years, there has been an increase in the number of events with a magnitude greater than  $M_w$  4.0 (up to 29.82 events per year). This increase could be related to the improvement of the Algerian seismological network (Yelles-Chaouche et al., 2007) and consequently to the improvement of the data quality, enabling the location of earthquakes with a magnitude in the range of 4.0 to 4.5.

In Peláez et al., (2018a, b), each area zone-source of the proposed seismogenic model has been characterized by different seismic parameters in order to compute its earthquake recurrence. They are the mean annual activity rate above magnitude  $M_w$  4.0, the  $b$ -value of the Gutenberg-Richter recurrence relationship, and the regional maximum earthquake magnitude  $m_{max}$ . In the present study, it is assumed that the distribution of the number of earthquakes with respect to their magnitudes follows the classical and well-known Gutenberg-Richter relation (Gutenberg & Richter, 1944). We used the estimated parameters calculated by Peláez et al., (2018a, b), using the Weichert method (Weichert, 1980). Thus, Fig. 2b displays for the studied area the non-cumulative and the truncated cumulative frequency. The estimated parameters are given by  $b = 0.78 \pm 0.08$  and  $a = 3.44 \pm 0.41$ . The maximum regional magnitude is estimated using a parametric approach. This method is widely used when a parametric model of the frequency-magnitude distribution is provided, as in the current study, where the classic Gutenberg-Richter relationship is assumed valid. Among the different methods described in Kijko (2004), Kijko and Singh (2011) and Kijko et al. (2016), we have used the Kijko-Sellevoll and Tate-Pisarenko estimators, based on the exact solution of Cook's generic equation (Cook 1979). Thus, the estimated value for the studied area is given by  $m_{max}^{K-S} = 7.67 \pm 0.62$  and  $m_{max}^{T-P} = 7.80 \pm 0.10$ , corresponding to Kijko-Sellevoll and Tate-Pisarenko estimators,



(a)



(b)

Figure 2

**a** Number of earthquakes above magnitudes  $M_W$  4.0, 5.0, 5.5 and 6.0 vs. time showing different completeness periods. **d** Cumulative and non-cumulative frequency of magnitude events above  $M_w$  4.0 for the studied area

respectively. These two estimated values are very close, and we consider that it is reasonable, in a conservative way, to adopt for the studied area the value  $m_{max} = 7.80 \pm 0.10$ .

### 3. Fault-Based Seismic Hazard

Since there are many faults within the defined area, the current work focuses on modeling the active faults that have already been reported. In this area, three primary faults were located and deemed active, as well as specified with accurate characteristics. They are the so-called Sahel, Blida, and Zemmouri Faults (see Fig. 1b). The Sahel and Blida Faults, respectively, describe the northern and southern borders of the Quaternary Mitidja Basin, whereas the Zemmouri Fault is located offshore, towards the northeastern edge. Several studies have looked into the Sahel anticline, such as that by Maouche et al. (2011), which looked at the uplift rate of the Sahel anticline and the uplift rate of the Zemmouri earthquake area. The slip-range derived through paleoseismological investigations by Heddar et al. (2013) is similar to the results obtained at the Sahel anticline. They also complement the previous study by Belabbes et al. (2009), which used joint inversion of interferometric synthetic aperture radar, coastal uplift, and GPS data to model the Zemmouri earthquake. Cetin et al. (2012) additionally give a detailed analysis of the deformation in the Zemmouri area by analyzing the InSAR time series covering 7 years of post-seismic deformation following the 2003 Zemmouri earthquake. The investigated area is also included in the seismogenic source zone model utilized by Sparacino et al. (2020) to relate to the geodetic deformation versus seismic crustal moment rates, deriving results in accord with those quoted previously.

It is worth noting, as seen previously, that the  $b$ -value for the entire zone has been estimated to be equal to  $b = 0.78 \pm 0.08$ . The previously described fault parameter data are used and converted into seismic hazard models, using the method described by Pace et al. (2016) and Visini et al. (2020). The procedure allows one to derive for each fault the maximum magnitude  $M_{max}$ , the mean recurrence time

Table 1

*The youngest and oldest year of occurrence for each recognized event at Sahel Fault, taken from Heddar et al. (2013)*

Interval range		
Event 1	1727	1779
Event 2	1455	1654
Event 3	1304	1365
Event 4	1171	1211
Event 5	778	897

$T_{mean}$  of the magnitude  $M_{max}$  and the seismic moment rate  $M_{orate}$ . Additionally, the  $b$ -value derived for the entire zone is used in the procedure, which computes the  $a$ -value to balance the total seismic moment rate with the seismic moment rate that was obtained by the pair  $M_{max}$  and  $T_{mean}$ . As pointed out by Pace et al. (2016), the obtained output file includes the annual rates for each magnitude bin above the threshold magnitude. The bin is an arbitrary choice, usually equal to 0.1.

Table 1 shows the paleoseismological data given by Heddar et al. (2013) for the considered Sahel Fault. As mentioned previously, these data were used to derive the mean recurrence time  $T_{mean}$  and its standard deviation  $\sigma_{T_{mean}}$  for that fault, following the procedures developed by Pace et al. (2016) and Visini et al. (2020). Accordingly, the CV (coefficient of variation) ratio, as defined by Peruzza et al. (2010), can be estimated as the following:  $CV = \sigma_{T_{mean}}/T_{mean}$ . Thus, the obtained

Table 2

*Mean recurrence time of  $M_{max}$*

	Mean return period	
	$T_{mean}$	Deviation
Arithmetic mean	238	CV = 0.51
Brownian Passage Time (BPT) distribution ( $\alpha = 0.42$ )	233	
Weibull (W) distribution ( $a = 267$ , $b = 2.58$ )	239	CV = 0.41
Poisson distribution	233	

CV corresponds to the coefficient of variation of  $T_{mean}$  for Sahel Fault

Table 3

*Fault parameters for each considered fault: length, dip, seismogenic thickness, SR1 and SR2 (minimum and maximum slip rate), maximum observed magnitude and its standard deviation, and last hosted event*

Fault parameters								
	Length (km)	Dip (°)	Depth (km)	SR1 (mm/year)	SR2 (mm/year)	Mo	$\sigma_m$	Last event
Sahel	63	45	12	0.1	0.3	6.5	0.1	1716
Zemmouri	43	45	14	0.3	0.6	6.9	0.1	2003
Blida	35	50	14	0.4	0.6	6.5	0.3	1825

arithmetic mean recurrence time for the Sahel Fault, was found to be equal to 240 years with a CV ratio equal to 0.51. Using the Brownian Passage Time (BPT) distribution (Matthews et al., 2002), it is equal to 230 years. The mean recurrence time was estimated to be equal to 240 years when using the Weibull distribution (Patel et al., 1976) with a CV ratio equal to 0.41, whereas when using the Poissonian distribution, it is equal to 230 years. The obtained results are summarized in Table 2. Using the tabulated fault parameters given in Table 3, i.e., the rupture fault length, the dip, the slip range, and the time of the last earthquake occurrence, the procedure used also allows the estimation of different maximum possible magnitudes. According to the IASPEI (2005) standard formula the MM0 magnitude is derived, the MRLD magnitude is estimated from the maximum subsurface fault length, the MRA magnitude is calculated from the maximum rupture area deduced from the empirical relationship of Wells and Coppersmith (1994), and the MAR magnitude, named magnitude aspect ratio by Pace et al. (2016), based

on the Peruzza and Pace (2002) aspect ratio relationship. Table 4 shows the results obtained for these magnitudes. Figure 3a–c draws a probability curve for each magnitude by following normal distributions that are symmetrically distributed around the central values.

The black dashed line in Fig. 3(a, b and c) represents the summed probability density curve, the vertical black line represents the central value of the Gaussian fit of the summed probability density curve, and the  $M_{\max}$  and its standard deviation  $\sigma_{M_{\max}}$  is given by the horizontal dashed line. The analysis carried out, as shown previously, allows deriving the magnitude distribution that each fault can generate. This is by modeling the seismicity rates with a truncated Gutenberg-Richter distribution. The distribution is truncated at both ends by the threshold magnitude  $M_c$ , considered equal to  $M_w$  4.0 and  $M_{\max}$ , but in this case the distribution is characterized by a smooth transition to  $M_{\max}$ , as defined and analyzed by Kagan (2002). The plots in Fig. 3d depict the magnitude distribution derived for each fault.

Table 4

*Maximum magnitude derived. MM0 from the standard formula (IASPEI, 2005),  $M_{\text{RLD}}$  from the maximum subsurface fault length,  $M_{\text{RA}}$  and  $M_{\text{AR}}$  are from both the maximum rupture area and using the Wells and Coppersmith (1994) relationship*

Maximum magnitude						
	MM0	$M_{\text{AR}}$	$M_{\text{RLD}}$	$M_{\text{RA}}$	Mobs	Mmax
Sahel	$7.12 \pm 0.30$	$6.78 \pm 0.25$	$7.17 \pm 0.26$	$7.06 \pm 0.25$	$6.50 \pm 0.10$	$7.00 \pm 0.30$
Zemmouri	$6.95 \pm 0.30$	$6.92 \pm 0.25$	$6.92 \pm 0.26$	$6.90 \pm 0.25$	$6.90 \pm 0.10$	$6.90 \pm 0.30$
Blida	$6.80 \pm 0.30$	$6.85 \pm 0.25$	$6.79 \pm 0.26$	$6.86 \pm 0.25$	$6.50 \pm 0.10$	$6.80 \pm 0.30$



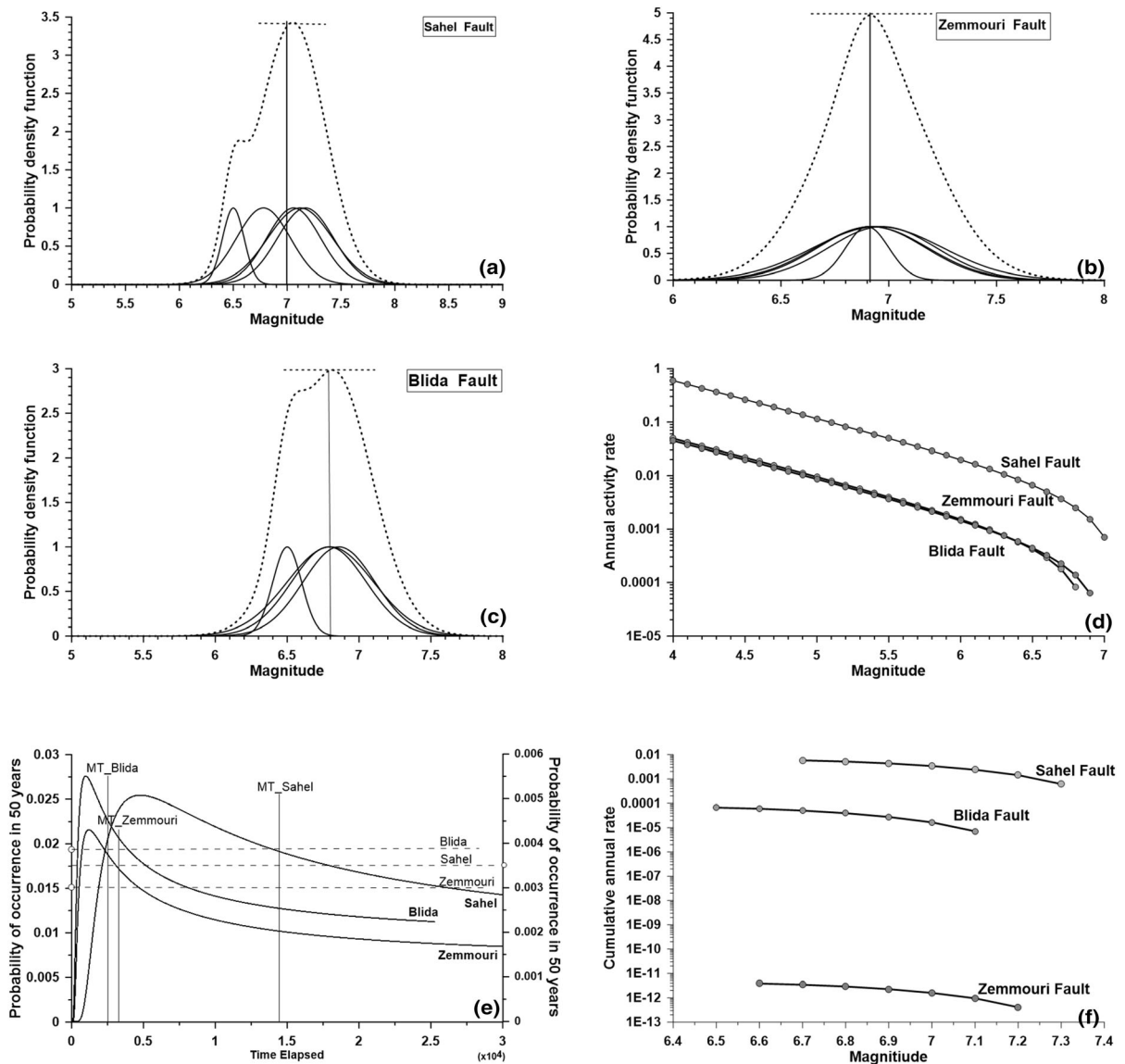


Figure 3

The summed probability density (PDF) curves in a dashed line for the (a) Sahel Fault, (b) the Zemmouri Fault and (c) the Blida Fault. (d) Truncated magnitude-frequency distribution of the Gutenberg-Richter for the three faults. (e) Probability of occurrence in 50 years of an earthquake in the interval  $M_{max} - \sigma$  and  $M_{max} + \sigma$  compared to the time elapsed since the last event for each fault in a dashed line, assuming that the behavior is Poissonian, and in a continuous line, assuming that the behavior is that of the so-called characteristic Gaussian Model. (f) Cumulative annual rate for the case of the characteristic Gaussian Model

As a result, the three active faults examined were characterized and considered as line source models, leading in the first proposed seismic source model in this study.

In order to perform the analysis of the seismic activity of the investigated faults, especially

considering both time-dependent and time-independent models, the appraisal of the probability of occurrence as a function of the time elapsed since the last event, is a requirement. To this end, the typical Gaussian model was endorsed, integrating the previously obtained results, leading to the results depicted

in Fig. 3e. In the case of the time-dependent model, the results depicted in Fig. 2f represent for the analyzed faults the probabilities of occurrence of magnitudes between  $M_{\max} - \sigma$  and  $M_{\max} + \sigma$ . The time-dependent probability of occurrence (solid line) is computed for the next 50 years, given an elapsed time since the last event (Fig. 3e); these probabilities were obtained using the BPT model. The second model, the time-independent distribution (dashed line), also refers to a period of 50 years. The vertical line in the plot also shows the mean recurrence time of magnitudes greater or equal to  $M_{\max} - \sigma$ . Thus, we can deduce that assuming the independent behavior of the elapsed time since the last event that is a Poissonian model, the obtained probabilities are equal to 0.0019, 0.015 and 0.0035 for the Blida, Zemmouri and Sahel Faults, respectively. In addition, the mean recurrence time for magnitudes equal or greater than the lower bound  $M_{\max} - \sigma$ , e.g., 6.5, 6.6 and 6.7 for Blida, Zemmouri and Sahel Faults, respectively, is estimated equal to 2525, 3275 and 14,450 years, and the time elapsed since the last event is 194, 16 and 304 years for these faults, respectively. The probability of exceeding the previous lower bound given the elapsed time for each fault is equal to 0.028, 0.022 and 0.0051, respectively. Figure 3f displays the cumulative annual rate of magnitudes within the range  $M_{\max} - \sigma$  and  $M_{\max} + \sigma$  obtained using the characteristic Gaussian model.

#### 4. Gridded Seismicity Model

It is common practice in probabilistic seismic hazard analysis (PSHA) to model the distributed or background seismicity as either a series of area sources in which each source is represented by a spatially uniform recurrence rate, or as a matrix of gridded seismicity sources with spatially smoothed recurrence rates (e.g., McGuire, 2004; Thenhaus & Campbell, 2003). It is worth noting that, as introduced by Frankel (1995) and Frankel et al. (2000), this approach has been used by several authors in different parts of the world (e.g., Lapajne et al., 2003; Peláez and López Casado, 2002; Peláez et al., 2003; Xu, 2019). According to Monelli et al. (2014), the expression “distributed seismicity”

encompasses all earthquake activity that cannot be associated with known and well-characterized fault structures. It is valid for any PSHA conducted, even in areas where an active fault inventory is available, because no fault inventory is ever complete. As a consequence, the distributed or background seismicity model is a reliable tool for regions that lack and/or have insufficient data on the different fault sources, as well as for regions where seismicity is not clearly associated to geological features (e.g., Frankel, 1995, 2000; Peláez and López Casado, 2002; Peláez et al., 2003, 2005a).

In this study, we used the gridded seismicity model, defined as a set of point sources. Each point is parameterized so that the rupture is represented as a three-dimensional planar rectangle. According to Monelli et al. (2014), the ruptures are generated at a single geographical location and can be distributed over multiple orientations, faulting styles, and depth levels. Rupture centroids are located at the point source location and are positioned at the depth specified by the hypocentral depth distribution. To avoid the rupture plane crossing the upper and lower boundary of the seismogenic layer, it is shifted along the dip direction so that it fits the upper and lower seismogenic depths. The rupture length is calculated using the Wells and Coppersmith (1994) relationships. The seismic hazard parameters of the zone-source model developed by Peláez et al., (2018a, 2018b) were smoothed using the Bender and Perkins (1987) procedure over gridded square cells. At each grid node, the  $a$  and  $b$  parameters of the Gutenberg-Richter relationship, as well as the maximum expected magnitude, were calculated. The truncated distribution of the Gutenberg-Richter relationship is used for magnitude events above  $M_w$  4.0 that occurred after 1925. The following is a summary of the methodology used. The number of earthquakes greater than  $M_w$  4.0 is counted, using the earthquake data file, within each square cell of  $0.1^\circ \times 0.1^\circ$  of a grid covering the studied area. Therefore, the annual number of earthquakes above magnitude  $M_w$  4.0 is derived using the Gutenberg-Richter relationship with the corresponding  $b$ -values derived for the studied area. Afterward, these values are spatially smoothed using a Gaussian filter (Frankel, 1995), given by

$$\bar{n}_i = \frac{\sum_{\Delta_{ij} \leq 3c}^j n_j \exp\left(-\frac{\Delta_{ij}^2}{c^2}\right)}{\sum_{\Delta_{ij} \leq 3c} \exp\left(-\frac{\Delta_{ij}^2}{c^2}\right)}, \quad (5)$$

In this relation,  $\bar{n}_i$  is normalized to preserve the total number of events and  $\Delta_{ij}$  is the distance between the  $i$ th and  $j$ th cells. The sum is taken over cells within a distance of  $3c$  of cell  $i$ . The parameter  $c$  is the parameter of the Gaussian filter, called the correlation distance. For each site, the values  $\bar{n}_i$  are binned by their distances from that sites, so that  $N_k$  denotes the total number of earthquakes that have taken place at a given cell, during a time interval  $T$  in which the catalog is believed to be complete above the minimum magnitude considered in the calculation. Thus, the rate of earthquakes with magnitude  $m_l$  in a cell at a distance  $r_k$  from the point of calculation is given by (Peláez and Lopez Casado, 2002)

$$\lambda(m_l, r_k) = \frac{N_k}{T} q(m_l, \Delta m). \quad (6)$$

The function  $q$  is the fraction of earthquakes in the interval of magnitude  $m_l \pm \Delta m$ , derived by using the truncated Gutenberg-Richter relationship,

$$q(m, \Delta m) = \frac{10^{-b(m-m_c)}}{1 - 10^{-b(m_{\max} - m_c)}} \left[ 10^{b\frac{\Delta m}{2}} - 10^{-b\frac{\Delta m}{2}} \right] \quad (7)$$

The chosen  $c$ -value takes into account the uncertainty in the earthquake location in the studied area over the time span of the catalog; in the current study, it is equal to 20 km, which is considered an optimal value by Peláez et al. (2016).

Using the described procedure, the gridded seismicity model for the current assessment is built using the resulting updated earthquake file previously discussed. Thus, the seismicity model is defined at the nodes for the  $0.1^\circ \times 0.1^\circ$  grid cell, which encompasses the area between longitudes  $1.5^\circ$  to  $4.0^\circ$  E and latitudes  $35.5^\circ$  to  $37.5^\circ$  N.

### 5. Selection of Ground-Motion Prediction Equations

The selection of the ground-motion prediction equations (GMPEs) is mainly dependent on the prevailing seismotectonic setting of the region and

on the availability of strong motion data. Considering that numerous equations have been proposed and published (Douglas, 2003), selecting appropriate GMPEs is a vital part of any seismic hazard analysis. The selection should not be based on purely geographic considerations (Bommer et al., 2010), since several studies have established that there is no persistent regional difference in ground motion among tectonically comparable areas (Douglas, 2007; Stafford et al., 2008). In the present study, we used the criteria initially introduced by Cotton et al. (2006) and updated by Bommer et al. (2010).

Most PSHA studies for northern Algeria (Peláez Hamdache, & Lopez Casado, 2003, 2006; Peláez, Hamdache, et al., 2005) used the GMPE by Ambrose et al. (1996), because their database included few data from Algerian earthquakes. Nevertheless, this GMPE was not suitable, since, among other reasons, it is expressed in terms of surface-wave magnitude ( $M_s$ ) and not moment magnitude (Kanamori, 1983). The GMPE by Laouami et al. (2018), which is based on Algerian strong-motion data and could have been an alternative, is unfortunately only described in terms of hypocentral distance and magnitude for rock, firm, and alluvial sites. Additional terms related to the effects of rupture physics, such as faulting style, fault dip, and rupture, are omitted in its simplified functional form. As a result, it will not be included in the current assessment.

Twelve prediction equation models were chosen as potential candidates for use in performing a seismic hazard assessment in the current study, following the recommendations provided by Cotton et al. (2006), Bommer et al. (2010), and Stewart et al. (2015). These models were chosen as they were developed for comparable seismotectonic settings, namely, active shallow crustal areas (Stafford et al., 2008). These models are the recent Pacific Earthquake Engineering Research Next Generation Attenuation (PEER-NGA) relationships developed by Campbell and Bozorgnia (2008, 2014), Abrahamson et al. (2014), Chiou and Youngs (2008, 2014), Idriss (2014), Boore and Atkison (2008) and Boore et al. (2014), denominated as CB08, CB14, ASK14, CY08, CY14, Idr14, BA08 and BSSA14, respectively. The four other candidates are those developed by Akkar

Table 5  
*Applicability range values for each GMPE*

GMPE	Magnitude range	Distance range
Akk_Bom_2010	5.0–7.6	Up to 100 km
CY08	4.0–8.5	Up to 200 km
CY14	3.5–8.0	Up to 300 km
Cauzzi_2015	4.5–7.9	Up to 150 km
Idr14	5.0–8.0	Up to 150 km
Fac_2010	5.0–7.2	Up to 150 km
Bind_2011	4.0–6.9	Up to 200 km
BA08	5.0–8.0	Up to 200 km
BSSA14	3.0–8.5	Up to 400 km
CB08	4.0–8.5	Up to 200 km
CB14	3.0–8.5	Up to 300 km
ASK14	3.0–8.5	Up to 300 km

and Bommer (2010), Faccioli et al. (2010) and Cauzzi et al. (2015), abbreviated as Akk\_Bom\_2010, Fac\_2010, Bind\_2011 and Cauzzi\_2015, respectively.

The first stage in the selection process is to determine the applicability range of each GMPE. The

one proposed by Akkar and Bommer (2010) is for distances up to 100 km and for earthquakes with magnitudes between 5.0 and 7.6. The Chiou and Youngs (2014) attenuation equation is considered as an update to the Chiou and Youngs (2008) model. The most recent one has a range of applicability larger than the previous one, covering distances up to 300 km and magnitudes between 3.5 and 8.0, whereas it is up to 200 km and magnitudes between 4.0 and 8.5 for the Chiou and Youngs (2008) attenuation equation. In the Chiou and Youngs (2014) model, some modifications have been introduced to the 2008 model, among them related to style of faulting, hanging wall effects, scaling with the depth to the top of the rupture, scaling with sediment thickness, and the inclusion of additional terms for the effects of fault dip and rupture directivity. The range of applicability of the Cauzzi et al. (2015) attenuation equation model covers distances up to 150 km and magnitudes between 4.5 and 7.9. This range is larger than in the Akkar and Bommer (2010) equation, but smaller than that of Chiou and Youngs (2014). Similarly, the range of applicability of Idriss (2014) and Faccioli et al. (2010) covers distances up

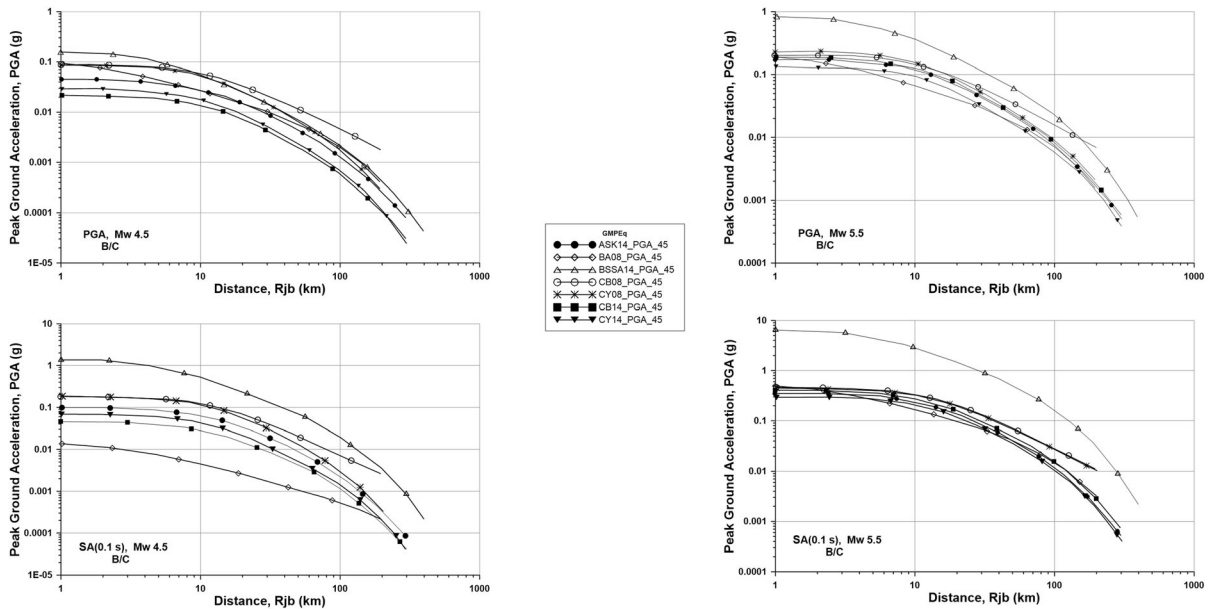


Figure 4  
 Plots of the selected GMPEs vs. distance Rjb for Mw 4.5 and Mw 5.5 in terms of PGA, SA(0.1 s) and SA(1.0 s)

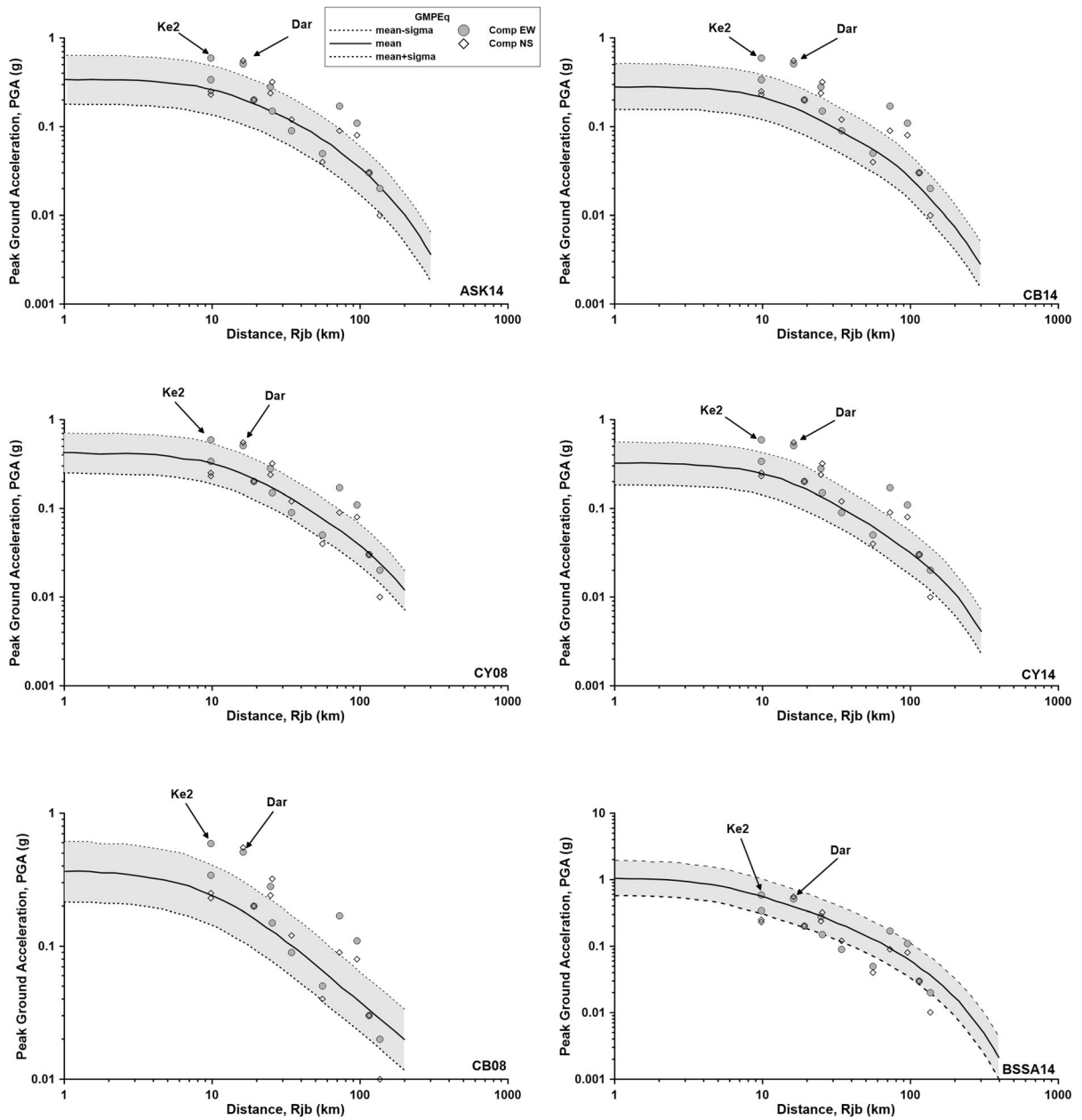


Figure 5

Plots of the mean PGA (solid line) and standard deviation (dashed lines) vs. the Rjb distance. The component EW and NS of the recorded acceleration during the 2003 Zemouri earthquake are shown in the plots, with the name of two stations Ke2 and Dar

to 150 km and a magnitude range between 5.0 to 8.0 and 5.0 to 7.2, respectively, whereas for Bindi et al. it covers distances up to 200 km and magnitudes ranging between 4.0 and 6.9. On the other hand, for the Boore and Atkison (2008) relationship, the range

of applicability covers distances up to 200 km and magnitudes between 5.0 and 8.0, whereas for Boore et al. (2014), named in this study BSSA\_2014, it covers distances up to 400 km and magnitudes between 3.0 and 8.5. Regarding the range of applicability of



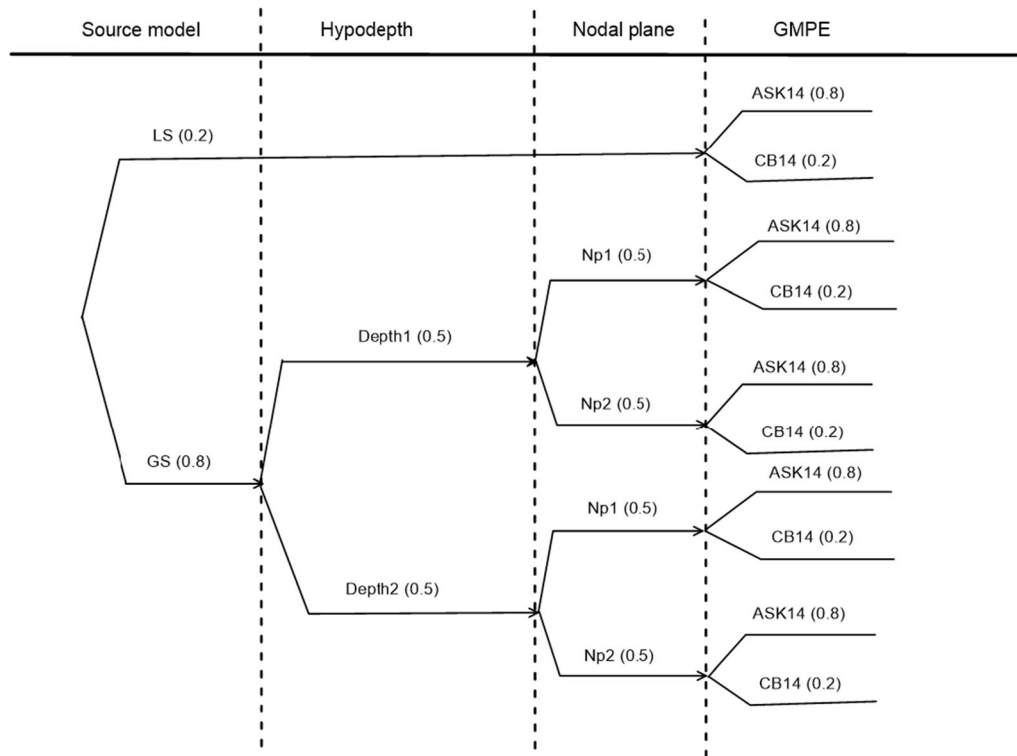


Figure 6

Logic tree used in this study. GS correspond to the gridded seismicity model, whereas LS correspond to the line-source model

the Campbell and Bozorgnia (2008) and Chiou and Youngs (2008) prediction equations, they cover distances up to 200 km and magnitudes between 4.0 and 8.5. For Abrahamson et al. (2014), Campbell and Bozorgnia (2014), and Chiou and Youngs (2014), it is larger, covering distances up to 300 km and magnitudes between 3.0 and 8.5 for the first two, and 3.5 to 8.0 for the third one. For the last model, developed by Boore et al. (2014), the range of applicability covers distances up to 400 km and magnitudes between 3.0 and 8.5. The applicability range values for each GMPE are given in Table 5.

According to the recommendation by Bommer et al. (2007) not to apply GMPEs outside their magnitude range, six ground-motion prediction equations are first identified, those of Abrahamson et al. (2014), Campbell and Bozorgnia (2008, 2014), Chiou and Youngs (2008, 2014) and Boore et al. (2014). The above-mentioned GMPEs have been compared for different earthquake scenarios; median predicted ground motion from the

six GMPEs for PGA and 5% damped spectral acceleration (SA) at 0.1 s are displayed in Fig. 4 for  $M_w$  4.5 and 5.5, respectively, assuming that the site type is B/C ( $V_s$  (30) equals 760 m/s). It can be observed that the variation of the median predicted values is wider for  $M_w$  4.5 than for  $M_w$  5.5. Furthermore, except for the BSSA14 and CB08 models, the GMPEs have similar median predicted amplitudes, especially for  $M_w$  5.5. The BSSA14 model predicts higher values, and the CB08 displays different behavior.

The GMPEs were compared to strong-motion recordings from the studied area. Figure 5 depicts the two horizontal components of recorded acceleration at 12 stations on May 21, 2003 ( $M_w$  6.9) during the Zemmouri earthquake, which are compared to predicted values by the six preselected GMPEs based on their applicability range. To appreciate and select the most appropriate GMPE, we use the horizontal components of the records from the 2003 Zemmouri earthquake, as analyzed

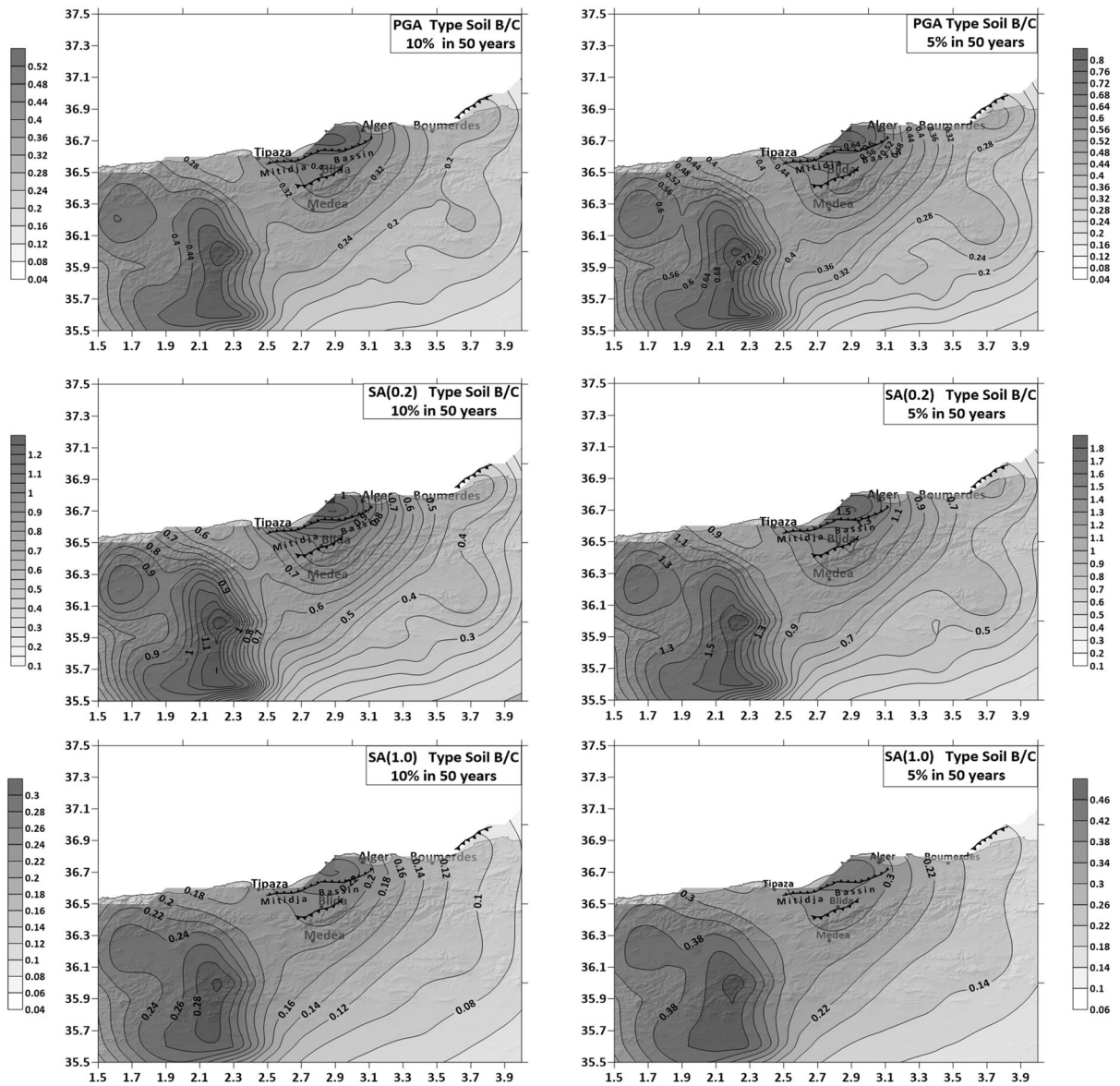
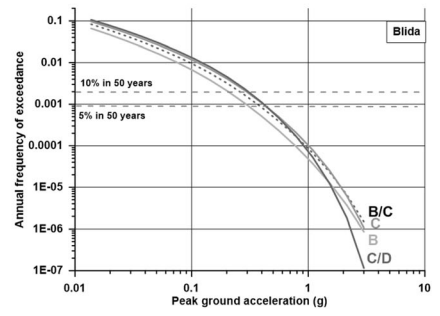
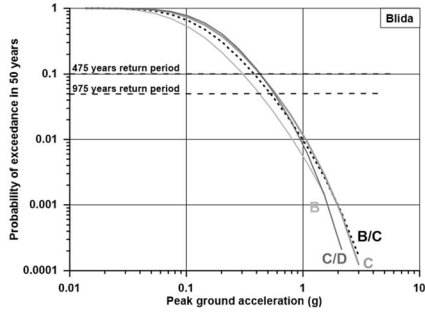
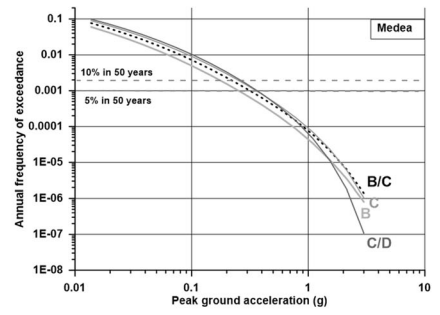
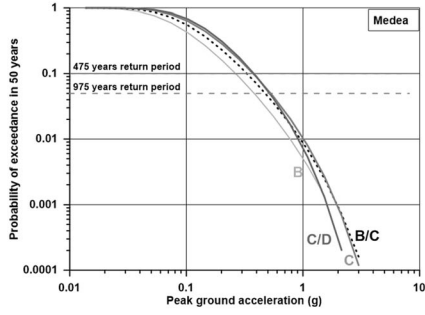
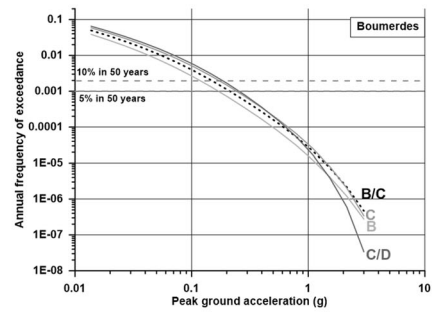
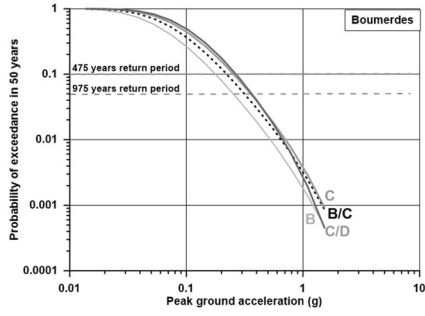
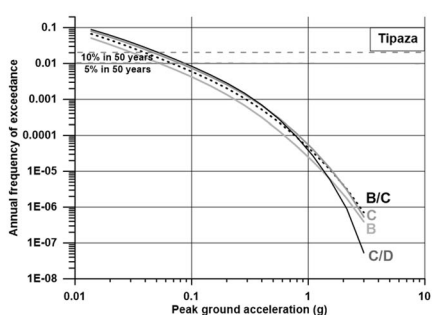
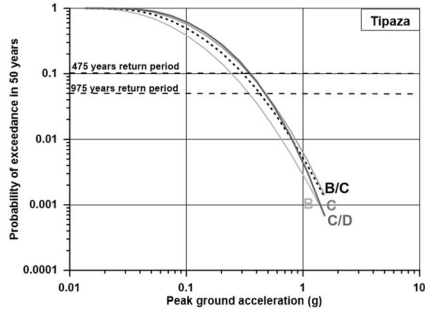
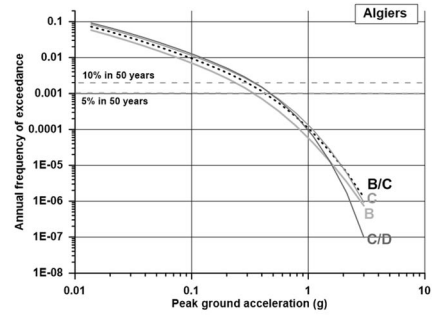
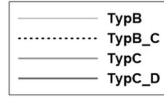
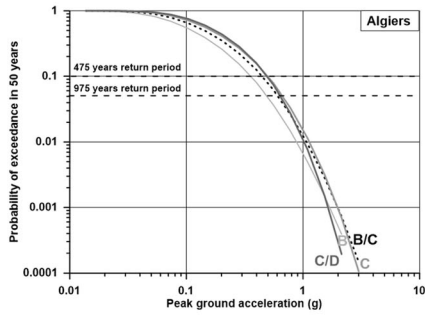


Figure 7

Seismic hazard maps in terms of PGA, SA (0.2 s) and SA (1.0 s) for B/C soil condition and for return periods of 475 and 975 years

by Peláez et al. (2006b). The CB08 and CY08, as depicted, have a range of up to 200 km. It can be seen that PGA values at the stations Ke2, equal to 0.59 g and 0.23 g for components EW and NS, respectively, and equal to 0.51 g and 0.55 g at station Dar, for EW and NS components, respectively, are not well constrained. According to Peláez et al. (2006b), these values result from the soil conditions, stiff soil for Ke2 and soft soil for

Dar station. These values are, in the case of the BSSA14 equation, in the range of mean plus/minus sigma, and close to the mean plus sigma values in the case of CY08. The CY14 seems to fit better with the component NS than with the component EW. Finally, the ASK14 and CB14 ground-motion prediction equations remain the best fit for the recorded accelerations, with the first being more accurate than the second. Furthermore, each GMPE



◀Figure 8

Seismic hazard curves and annual frequency of exceedance in terms of PGA for B, B/C, C and C/D soil conditions

has a similar range of applicability. As a result, we chose the ASK14 and CB14 GMPEs because they are considered sufficiently robust to cover a wide range of magnitudes, distances, and spectral periods. It is worth noting that Bozzoni et al. (2011) presented this kind of comparison as a technique for weighing the GMPE considered in their assessment utilizing accelerometric data file covering the period from 1997 to 2008.

### 6. Logic Tree Framework and Seismic Hazard Computation

The seismic hazard evaluation in the current study was carried out using the previously discussed seismicity models. The first, known as the line-source model, is derived from the fault-based seismicity model, abbreviated as LS, and is based on the characteristics of three faults: the Blida, Zemmouri, and Sahel Faults. As shown in Fig. 3d, the truncated Gutenberg-Richter magnitude distribution was preferred to interpret the frequency of earthquakes with magnitudes greater than Mw 4.0 for these faults. The gridded seismicity model previously described and denoted as GS is the second complementary model. The empirical models provided by the specified GMPEs, namely the ASK14 and CB14 models, are used to estimate the ground-motions produced by future occurrences.

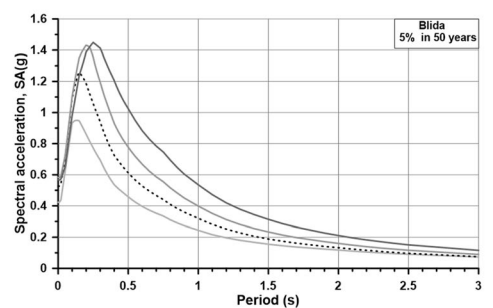
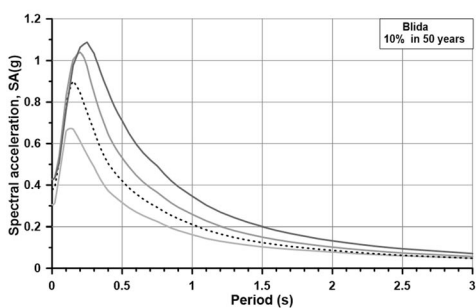
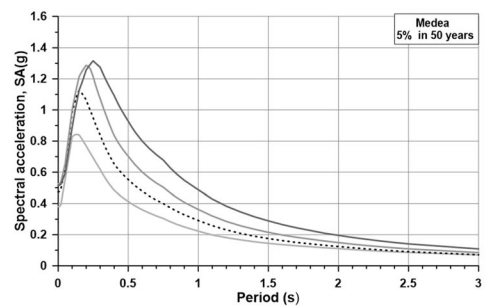
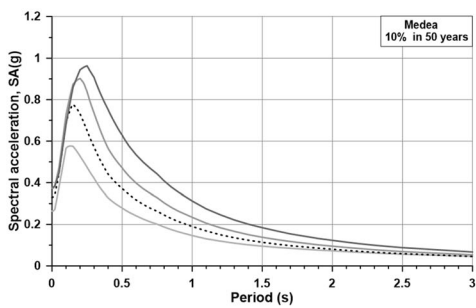
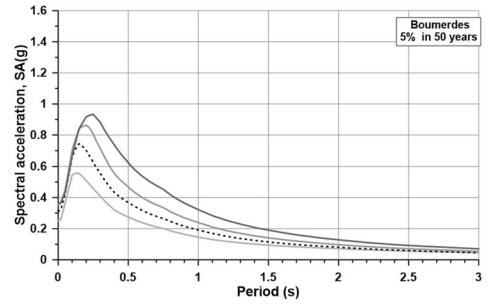
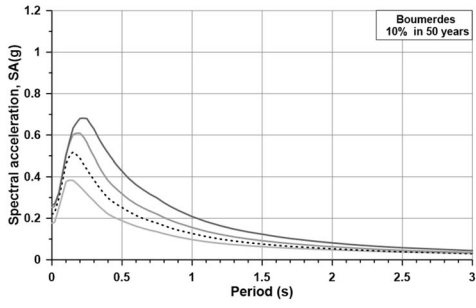
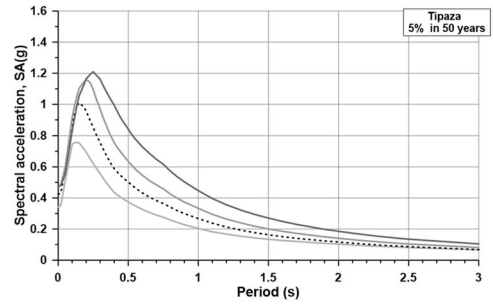
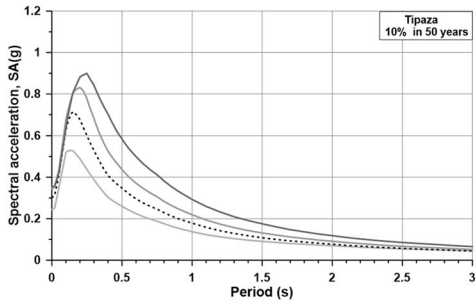
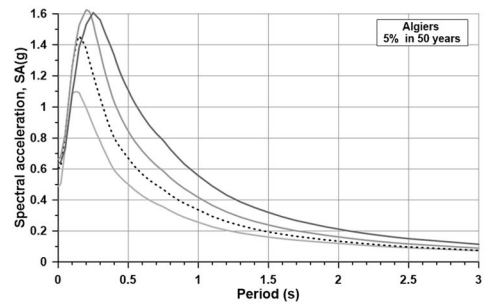
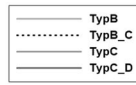
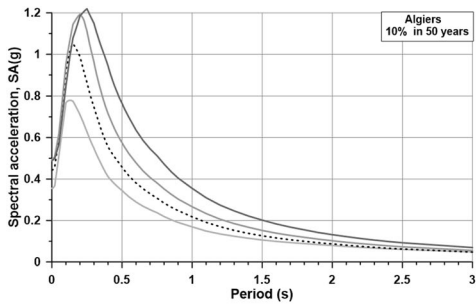
A logic tree scheme is the most commonly and widely used tool for capturing epistemic uncertainty in the most widely used seismicity model (Bommer & Scherbaum, 2008; Kulkarni et al., 1984). According to Bommer et al. (2005), including more than one GMPE in the logic tree assessment is a standard procedure for appreciating the epistemic uncertainty in selected ground-motion attenuation models. Thus, the epistemic uncertainties in the current study were addressed in a logic tree framework by considering the following parameters: (a) the line source and

gridded seismicity source models, denoted LS and GS, (b) the hypo-depth, (c) the nodal planes, and (d) the GMPEs. We assert that, for a seismic hazard assessed for a short return period, the contribution of the fault model, despite its long return period, is lower than that of the gridded seismic model solely based on the earthquake catalog. The fault model should contribute more than gridded seismicity when assessing seismic hazard for a relatively long return period. As result, a weight equal to 0.80 is considered for the gridded model used in the ongoing study, whereas it is considered equal to 0.20 for the linear source model (LS). Hamdache et al. (2010) and Pelaez et al. (2018 a, b) describe the seismogenic depth as being between 0 and 15 km. The proposed GS model took into account two seismicity depths of 4 and 8 km, each with the same weight. Furthermore, the consideration of two distinct nodal planes agrees with the orientations of the SHmin and SHmax previously obtained by Peláez et al. (2018a, 2018b). In this study, the same weight is assigned to both nodal planes because there is no reason to prefer one to the other.

A weighted procedure is required following the selection of the GMPEs. In general, the weighting procedure is supported by extensive judgments and opinions, so a group of experts assigns each GMPE's weight subjectively. However, subjectivity is currently a target of PSHA criticism, and scientists' goal is to reduce subjectivity as much as possible. In this context, Scherbaum et al. (2009) introduced a weighting scheme based on scoring the GMPEs, that is, a numerical evaluation of how well each GMPE fits a set of data. In classical information theory, this procedure is established on the likelihood that it is related to information loss, assuming that the data are independent. The proposed scoring scheme is based on the average log likelihood; for one specific model, this result in the expression

$$LLH_k = -\frac{1}{N} \sum_{i=1}^N \log_2 \{f(x_i)\}, \quad (8)$$

with  $x_i$ ;  $i = 1, 2, \dots, N$  a given set of ground-motion observations. In the previous relationship,  $f(x)$  is a probability density function describing the GMPE,  $x$  is the random variable described by the





◀Figure 9

Computed uniform hazard spectra at each city, damped at 5%, for return periods of 475 and 975 years, and for B, B/C, C and C/D soil conditions

GMPE that has a truncated Gaussian distribution given by

$$f(x) = \frac{1}{\sigma\sqrt{2\pi}} \exp \left[ -\frac{(x - \mu)^2}{2\sigma^2} \right] ; \quad x \leq x_0, \tag{9}$$

in which  $\mu$  is the mean and  $\sigma$  the standard deviation of the Gaussian distribution, and  $x_0$  is the truncation point, usually given by  $x_0 = \mu + 3\sigma$ . The LLH estimator is utilized as a criterion to classify the GMPEs that have been chosen. The lower the LLH, the closer the candidate model is to the process that produced the data; the higher the LLH, the less likely the model is to have produced the data. Scherbaum et al. (2009) provide the relative weight

of the  $k$ th GMPE model; in a set the  $K$  models, it is given by

$$w_k = \frac{2^{-LLH_k}}{\sum_{j=1}^K 2^{-LLH_j}}. \tag{10}$$

Because the procedure is simple and has the advantage of indicating the model's relative performance with a single score, the ranking method is now one of the most widely used data-driven evaluation methods among many researchers. It has been used by Delavaud et al. (2012b) in Europe in the frame of the SHARE project and in California (USA) to test the global applicability of GMPEs for active shallow crustal regions (Delavaud, Scherbaum, et al., 2012), whereas Beauval et al. (2012) used it to test the GMPEs against small-magnitude data. It is worth noting that it was effectively used by Maiti et al. (2017) to select the appropriate GMPEs for PSHA purposes in the Indian region. An extension of the LLH method is proposed by Mak et al. (2017) by introducing the multivariate logarithmic score approach. However, Kale and Akkar (2017)

Table 6

Seismic hazard values (g) obtained at the five main cities located in the studied area

Seismic hazard values											
City	Type	10% in 50 years					5% in 50 years				
		PGA	0.2SA	1.0SA	S <sub>Amax</sub>	T <sub>max</sub>	PGA	0.2SA	1.0SA	S <sub>Amax</sub>	T <sub>max</sub>
	B	0.355	0.710	0.169	0.779	0.13	0.489	0.993	0.256	1.095	0.12
Algiers	B/C	0.443	0.988	0.218	1.050	0.15	0.606	1.372	0.336	1.455	0.15
	C	0.495	1.193	0.266	1.193	0.20	0.664	1.624	0.416	1.624	0.20
	C/D	0.498	1.184	0.355	1.219	0.25	0.636	1.530	0.557	1.593	0.24
Tipaza	B	0.243	0.488	0.137	0.529	0.13	0.342	0.679	0.203	0.757	0.13
	B/C	0.305	0.676	0.178	0.714	0.15	0.425	0.956	0.267	0.993	0.17
	C	0.344	0.831	0.219	0.831	0.20	0.473	1.158	0.333	1.158	0.20
Boumerdes	C/D	0.352	0.881	0.292	0.898	0.25	0.471	1.163	0.446	1.209	0.25
	B	0.176	0.352	0.097	0.383	0.13	0.252	0.509	0.145	0.556	0.13
	B/C	0.221	0.488	0.126	0.517	0.15	0.314	0.701	0.191	0.744	0.15
Medea	C	0.253	0.608	0.155	0.609	0.19	0.355	0.863	0.239	0.863	0.20
	C/D	0.265	0.679	0.184	0.681	0.22	0.363	0.917	0.322	0.933	0.25
	B	0.264	0.527	0.146	0.576	0.13	0.380	0.768	0.222	0.842	0.13
Blida	B/C	0.330	0.732	0.189	0.776	0.15	0.473	1.063	0.291	1.116	0.16
	C	0.373	0.902	0.234	0.902	0.20	0.527	1.287	0.319	1.287	0.20
	C/D	0.379	0.944	0.312	0.963	0.25	0.515	1.257	0.487	1.316	0.25
Blida	B	0.304	0.610	0.162	0.672	0.13	0.423	0.859	0.244	0.950	0.13
	B/C	0.380	0.845	0.209	0.900	0.15	0.526	1.185	0.320	1.258	0.15
	C	0.427	1.038	0.258	1.038	0.20	0.582	1.431	0.398	1.431	0.20
	C/D	0.429	1.062	0.346	1.087	0.25	0.567	1.388	0.535	1.449	0.25

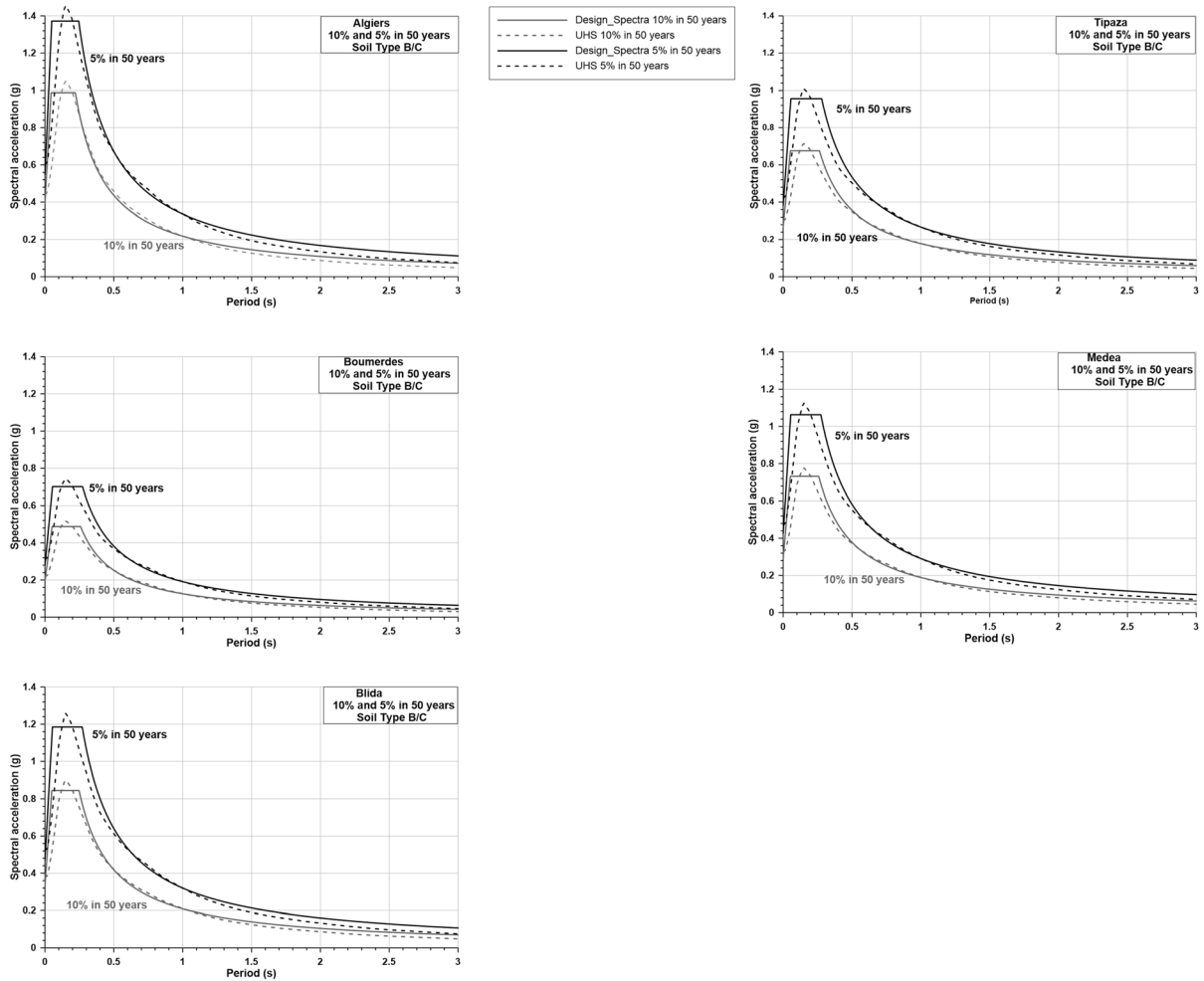


Figure 10

Uniform hazard spectra and design spectra, damped at 5%, for B/C soils and for return periods of 475 years and 975 years at each studied city

introduced a method named EDR based on the Euclidean distance, instead of maximum likelihood. Worthy of note also that Roselli et al. (2016) discuss a general probabilistic framework to numerically score and weight GMPEs. The Bayesian tools have been used by Arroyo et al. (2014) to assign weights to GMPEs, and Yazdani et al. (2021) show that these tools allow for merging information gathered from available seismic data and expert opinion.

The two selected GMPEs, ASK2014 and CB2014, have been ranked using the LLH procedure. The obtained results using the recorded accelerations during the 2003 Zemmouri (Algeria) earthquake are equal to

$$\begin{aligned} LLH_{ASK} &= -1.4114 \\ LLH_{CB} &= -0.6573, \end{aligned} \quad (11)$$

The resulting weights are

$$w_{ASK} = 0.6278 \simeq 0.63, \quad w_{CB} \quad (12)$$

According to Delavaud et al. (2012b), the calculated weights must be used to aid decision-making by providing additional information about the applicability of GMPEs, especially in regions like the one studied here where no specific model exists and because, in most cases, local records are not only insufficient but also scarce, rendering data-driven methods unreliable, justifying the use of

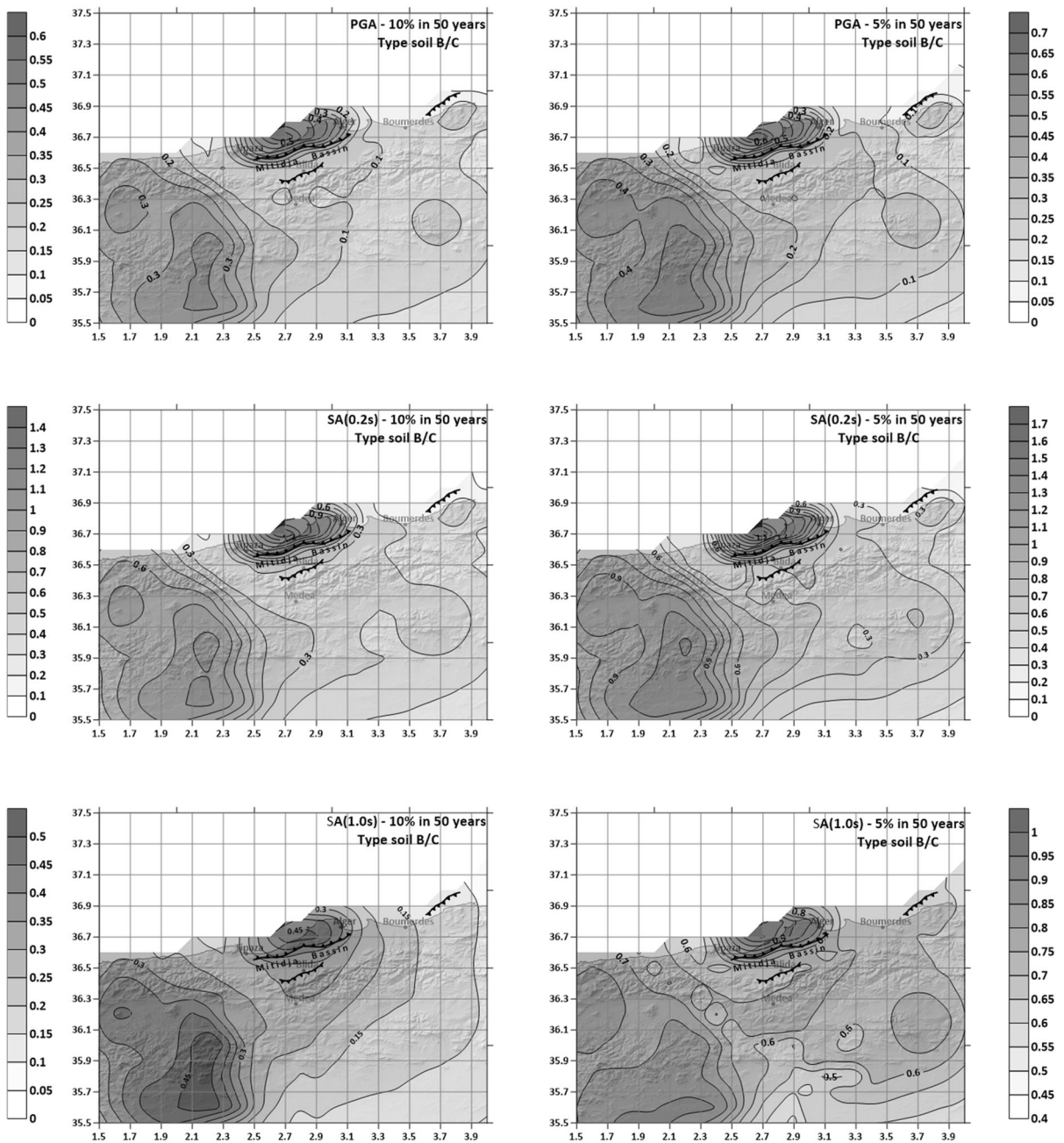


Figure 11  
The overall 95% confidence band maps for PGA, SA(0.2 s) and SA(1.0 s) for 475- and 975-year return periods

both experts' opinions and seismic data to assess the applicability of GMPEs, as processed by Secanell et al. (2018). In this context, according to our appreciation of the robustness and the range of

applicability of the selected GMPEs, the following weights are attributed to the selected GMPE models

$$w_{ASK} = 0.80 \quad , \quad w_{CB} = 0.20, \quad (13)$$

Table 7

<i>Degree of reliability for different values of the parameter COV</i>	
Range	Degrees of reliability
$0.0 \leq cov \leq 15\%$	Very high
$15\% \leq cov \leq 25\%$	High
$25\% \leq cov \leq 35\%$	Medium
$35\% \leq cov \leq 45\%$	Low
$Cov \geq 45\%$	Very low

Figure 6 presents the logic tree used, as well as its related corresponding weights. Two branches are associated with the LS model and eight branches with the GS model.

In the ongoing study, seismic hazard assessment was performed using the OpenQuake software (Pagani et al., 2014). The procedure adopted in OpenQuake, the classical PSHA (Field et al., 2003), is described in detail by Crowley et al. (2011). We have considered the level of truncation of the Gaussian distribution of the logarithm of ground motion used in the calculation of hazard equal to  $3\sigma$  and the maximum integration distance equal to 300 km. This distance has been chosen in adequacy with the applicability range of the selected GMPEs, referring to the largest distance between a rupture and the target calculation sites in order for the rupture to be considered in the PSHA calculation. By dividing the studied area into squared cells, as was quoted before, at each node of the grid, the ground-motion parameters (PGA and SA) with 10% and 5% probability of being exceeded in 50 years (corresponding to return periods of 475 and 975 years) were estimated for the selected soil types B, B/C, C and C/D (NEHRP site conditions). Figure 7 shows for the studied area the mean peak ground acceleration (PGA) maps, the estimated values for SA (0.2 s) and SA (1.0 s) damped at 5%, for 10% probability of being exceeded in 50 years for the B/C soil condition. We can observe three main clouds on each individual hazard map. The first one, in terms of hazard values, is located around the Mitidja Basin, and compiling the higher estimated values, reaches a PGA value of about 0.44 g and 0.61 g at the city of Algiers for return periods of 475 and 975 years, respectively, for the B/C soil condition. The second focus is located to the

southwest of Medea city, with lower values, and the third one is also located to the southeast of this city.

It is interesting to point out that at Algiers city the PGA value equal to 0.44 g is expected for a return period of 475 years and for soil condition B/C. This indicates that the mean value of the ground motion is obtained, for example, by replacing the real sequence of earthquakes in this area by a sequence of two earthquakes in 475 years, as each provides us this value of PGA. This is the basis of the methodology proposed by Joyner and Fumal (1985) for seismic hazard determination. An earthquake generating a PGA equal to 0.44 g should have a macroseismic intensity of VIII-IX, using the relationship between PGA and the macroseismic intensity by Murphy and O'Brien (1977), given in Linkimer (2008) by

$$I_{MM} = 2.86 \log(PGA) + 1.24 \quad , \quad (14)$$

$$IV < I_{MM} < X.$$

According to Maouche et al. (2011) and Harbi et al. (2015), during the last 475 years, two earthquakes with these characteristics took place in the studied area, those of 1716, February 3 ( $I_0$  IX), located offshore of Algiers, and the one that occurred on 1722, November 29 ( $I_0$  VII-VIII), located in Algiers. Similarly, the estimated PGA for a return period of 975 years, equal to 0.61 g, corresponds to a macroseismic intensity of about IX-X. This procedure highlights the reliability of the derived values.

The seismic hazard curves in terms of PGA with a 10% probability of exceedance in 50 years are derived for the selected sites, Algiers, Tipaza, Boumerdes, Medea, and Blida city, and for the mentioned soil types. Figure 8 exhibits the plots of the obtained results, revealing the annual frequency of exceedance, in terms of PGA, for the selected cities. The uniform hazard spectra (UHS) performs an appropriate probabilistic representation of earthquake action and is a key element in recent seismic design codes, such as the International Building Code (ICC, 2009), because it is an efficient way of describing a building's or structure's seismic hazard and ground-motion demand (Wen, 2004). The UHS is a standard PSHA output that is regarded as an important component of modern earthquake engineering and structural dynamics. It represents the joint effect of

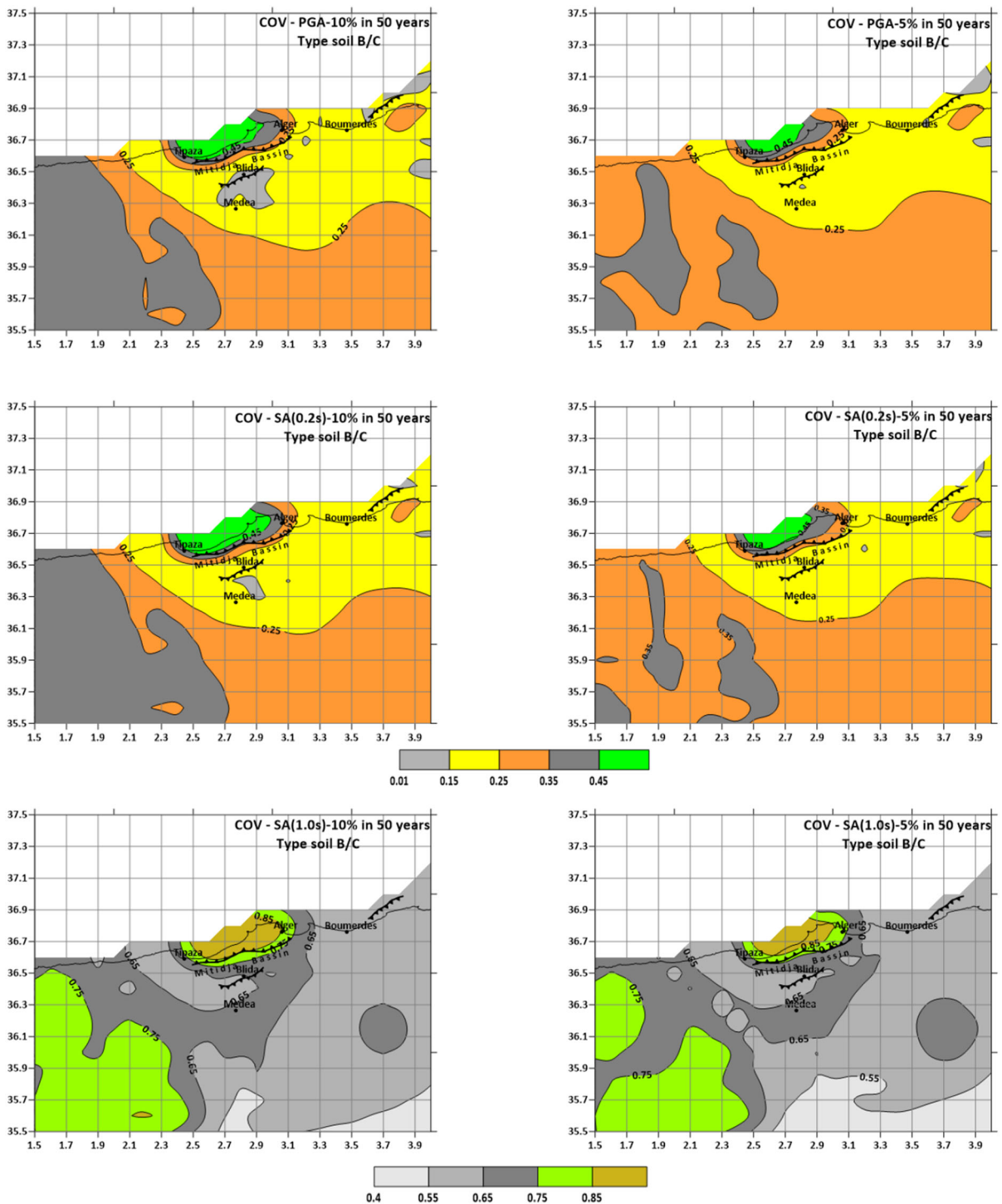


Figure 12

Maps showing the degree of reliability for PGA and SA (0.2 s) for 475- and 975-year return periods in terms of very high, high, medium, low and very low. For SA (1.0 s), the maps display the spatial variation of the COV for the two return periods



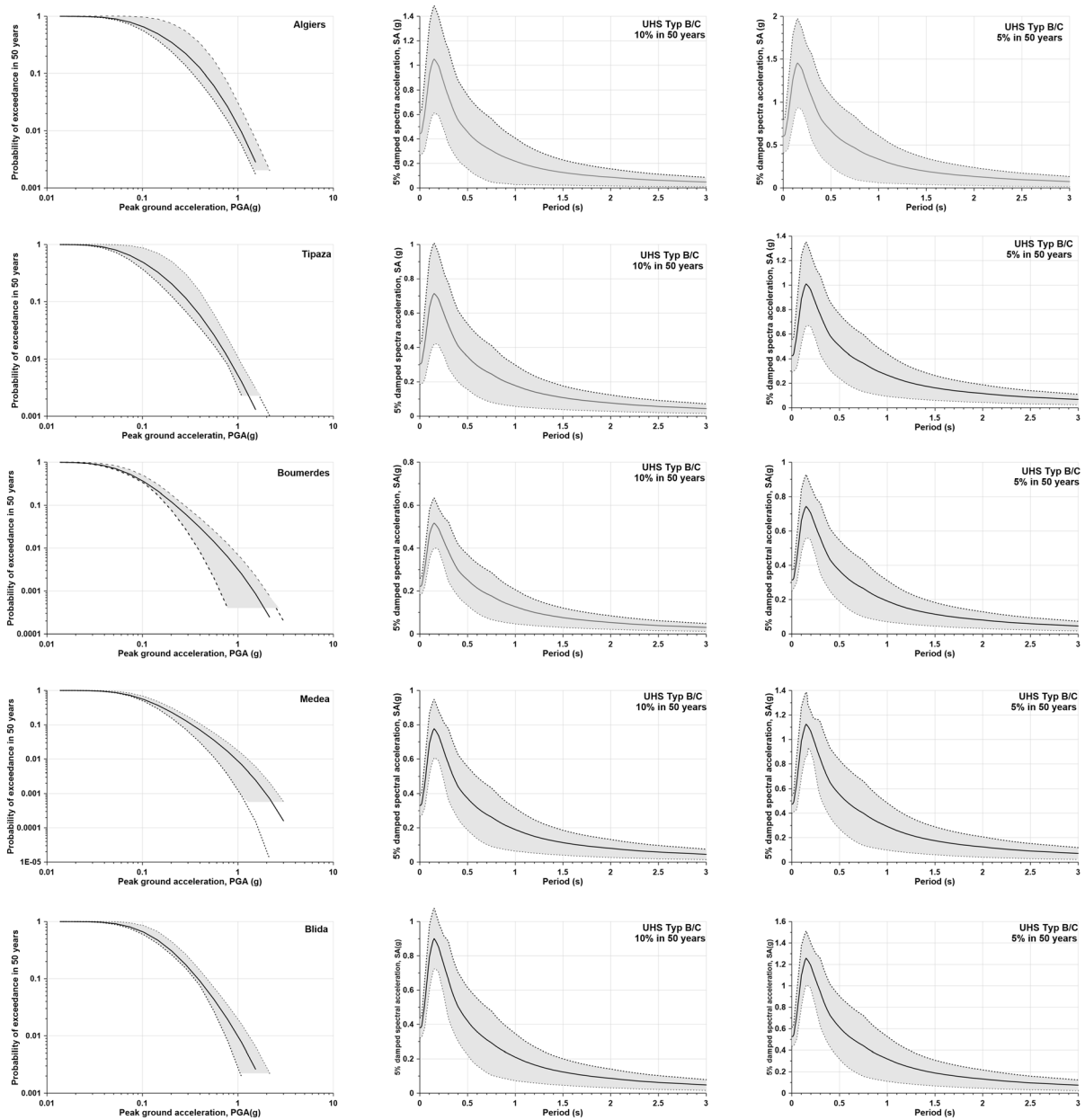


Figure 13

Plots depicting the seismic hazard curve at each studied city with the 95% confidence bands. The mean UHS (in solid line) and mean UHS  $\pm$  standard deviation (in dashed lines) are displayed

earthquakes of different magnitudes and source-to-site distances; the low-period part of the UHS is mainly controlled by the contribution of small to moderate-magnitude earthquakes from nearby seismic sources. Whereas the largest earthquakes that occurred at distant sources from the studied site affect

the large period part (over 0.5 s). Figure 9 depicts the uniform hazard spectrum (UHS) computed for each city for soil types B, B/C, C, and C/D, as well as return periods of 475 and 975 years. From the computed UHS for the selected return periods and soil types, useful engineering parameters are derived,

Table 8

*Peak ground acceleration and its standard deviation for the two selected return periods and soil conditions at the considered cities*

Peak Ground Acceleration and standard deviation			
City	Type	PGA with 10% in 50 years	PGA with 5% in 50 years
Algiers	B	$0.36 \pm 0.11$	$0.49 \pm 0.14$
	B/C	$0.44 \pm 0.17$	$0.61 \pm 0.19$
	C	$0.50 \pm 0.12$	$0.66 \pm 0.12$
	C/D	$0.50 \pm 0.10$	$0.64 \pm 0.10$
Tipaza	B	$0.24 \pm 0.07$	$0.34 \pm 0.09$
	B/C	$0.31 \pm 0.12$	$0.43 \pm 0.13$
	C	$0.34 \pm 0.18$	$0.47 \pm 0.07$
	C/D	$0.35 \pm 0.08$	$0.47 \pm 0.07$
Boumerdes	B	$0.18 \pm 0.03$	$0.25 \pm 0.05$
	B/C	$0.22 \pm 0.03$	$0.31 \pm 0.04$
	C	$0.25 \pm 0.02$	$0.36 \pm 0.03$
	C/D	$0.27 \pm 0.02$	$0.36 \pm 0.03$
Medea	B	$0.26 \pm 0.05$	$0.38 \pm 0.08$
	B/C	$0.33 \pm 0.06$	$0.47 \pm 0.07$
	C	$0.37 \pm 0.03$	$0.53 \pm 0.04$
	C/D	$0.38 \pm 0.03$	$0.52 \pm 0.04$
Blida	B	$0.30 \pm 0.06$	$0.42 \pm 0.08$
	B/C	$0.38 \pm 0.06$	$0.53 \pm 0.09$
	C	$0.43 \pm 0.03$	$0.58 \pm 0.04$
	C/D	$0.43 \pm 0.03$	$0.57 \pm 0.04$

which are tabulated in Table 6. The derived values of SA (0.2 s) and SA (1.0 s) for the selected soil types and the considered return periods were used to perform an earthquake-action analysis following current seismic design codes, in the form of absolute acceleration, or what is called the design response spectrum. According to the International Building Code (ICC, 2009), the SA (0.2 s) and SA (1.0 s) values are used to establish the spectral regions controlled by acceleration and velocity, respectively; the two values are clearly representative of the overall shape of the UHS. In the prevalent analysis performed in this study, the procedure developed by Malhotra (2005), based on the Newmark–Hall approach (Newmark & Hall, 1982), for the establishment of a design spectrum is used. The procedure was established to derive the so-called control period ( $T_s$ ), which can be easily estimated using the SA (1.0 s) and SA (0.2 s) values that were previously derived from the UHS.

$$T_s = \frac{SA(1.0s)}{SA(0.2s)} 1s. \quad (15)$$

Then, according to Malhotra (2005), the design spectrum values are obtained using the following relationship.

$$SA(T) = \begin{cases} 0.4 SA(0.2s) + 3 SA(0.2s) \frac{T}{T_s}; & T \leq 0.2 T_s \\ SA(0.2s); & 0.2 T_s < T \leq T_s \\ SA(1.0s) \frac{1.0s}{T}; & T > T_s \end{cases} \quad (16)$$

The calculated UHS and the derived design response spectra for both return periods (475 and 975 years) and soil type B/C are shown in Fig. 10. Regardless of return period or soil type, there is good agreement between the computed UHS and the established design spectra for the selected cities. The same results can be derived for soil conditions B, C, and C/D and selected return periods.

Thus, the derived Newmark–Hall design presents some advantages, it is soil type dependent, not only based on the characteristic period, but also on the hazard level, represented by the level of the constant spectral acceleration branch. Contrary to the current Algerian building code (Belazougui, 2017), which does not propose an elastic design spectrum for each individual site.

Figure 15  
Disaggregation of seismic hazard at studied cities in terms of PGA with 10% and 5% probability of exceedance in 50 years for a B/C soil type. The contribution of each computation cell is depicted (disaggregation in azimuth)

7. Uncertainty Analysis

This section is an attempt to investigate the overall uncertainty in the estimated seismic hazard

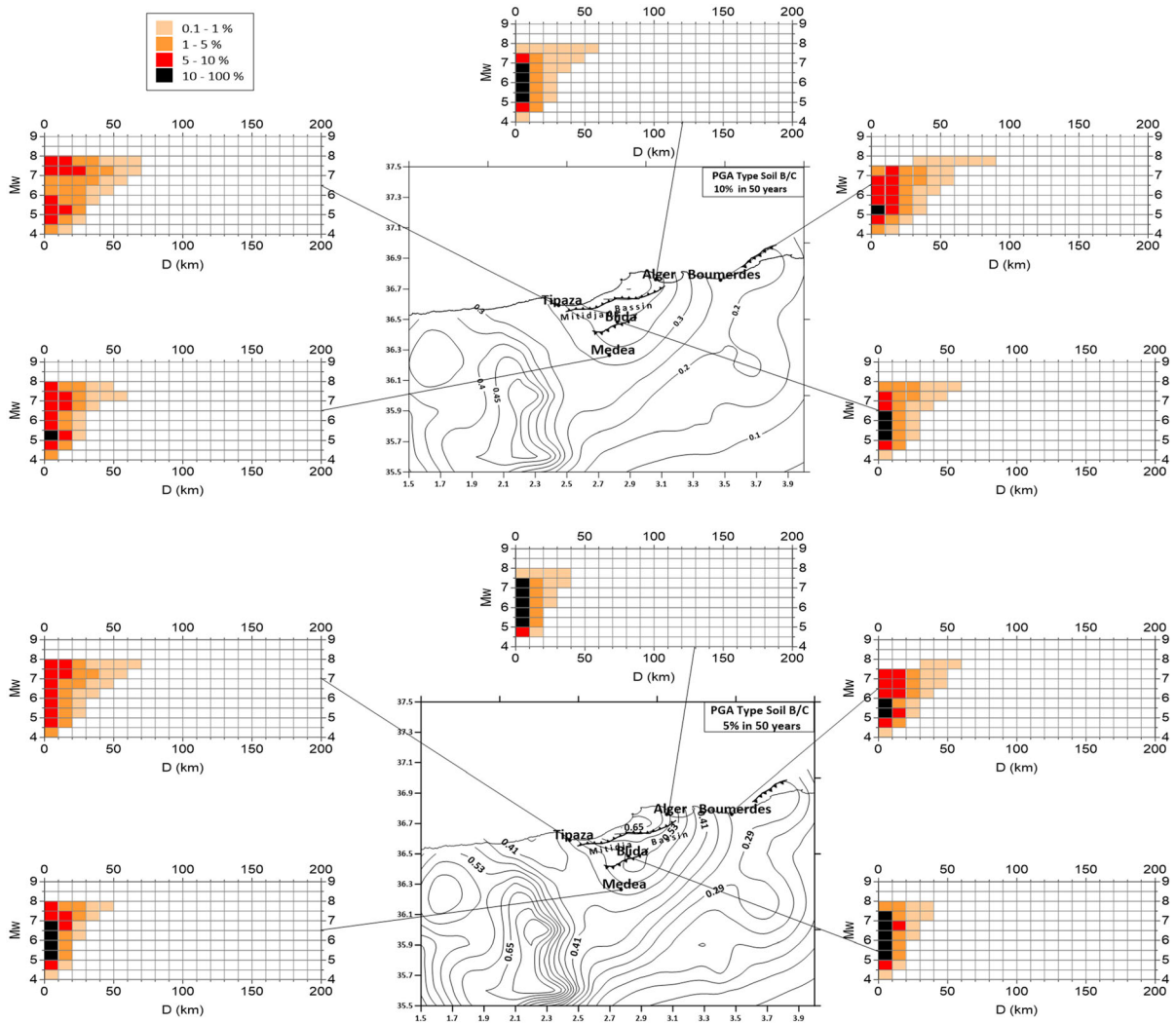
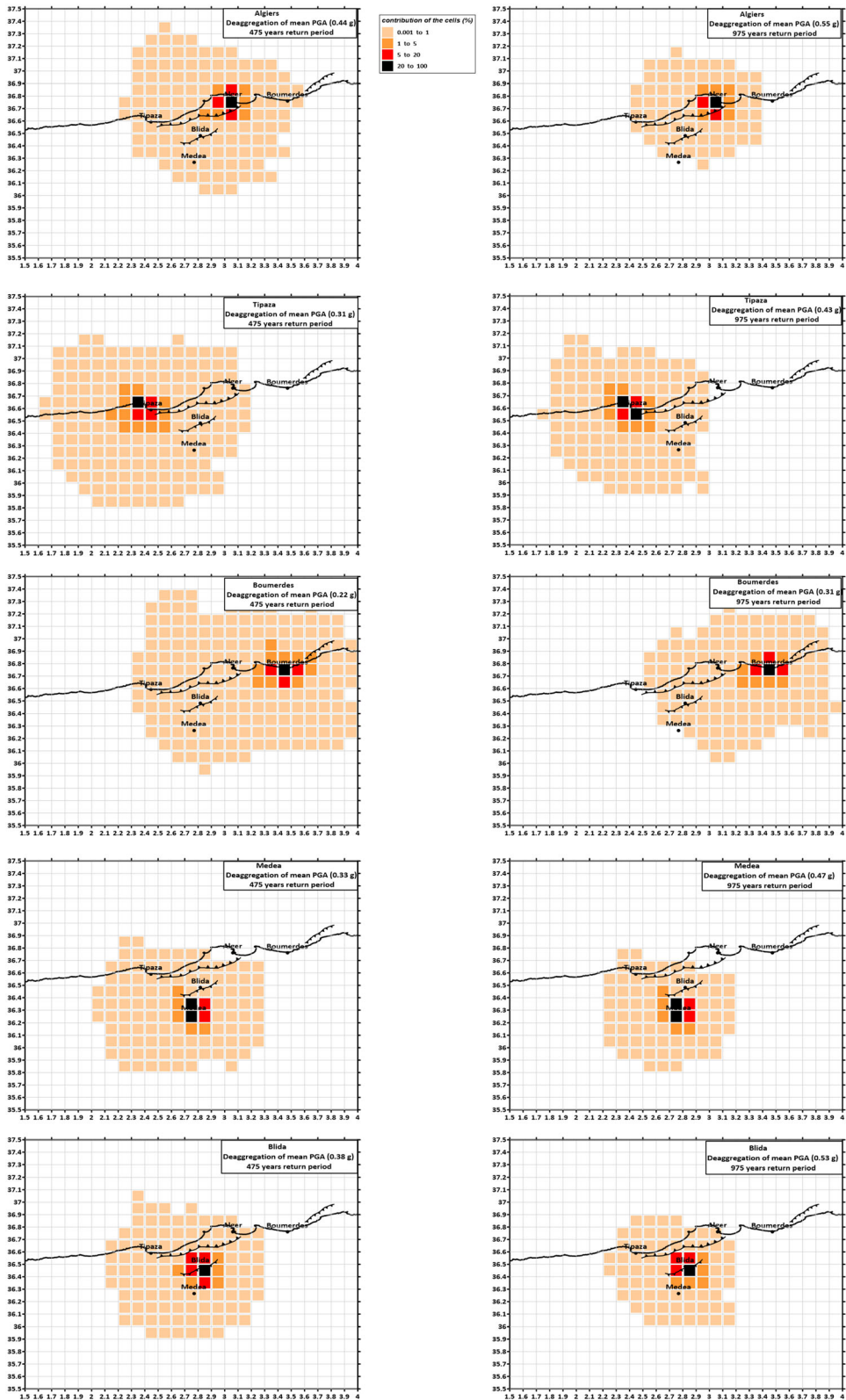


Figure 14

Seismic hazard disaggregation at studied cities in terms of PGA with 10% and 5% probability of exceedance in 50 years for a B/C soil type, and contribution of  $(M, D)$  pairs at each studied city



values. According to Lombardi et al. (2005), the first quantitative results on this topic were published by McGuire (1977) and McGuire and Sheldock (1981). Cramer et al. (1996), Cramer (2001), and Cramer et al. (2002) provide a detailed description of the methodology for assessing overall uncertainty in hazard assessment.

The conducted uncertainty analysis, as described by Atkison et al. (2014), is linked to the branches of the logic tree ground-motion attenuation relationship, with the goal of dealing with epistemic uncertainty. The uncertainties associated with the other parameters that define the two seismic models, as well as the two branches (hypocenter and nodal plane) of the GS model, are omitted. A sensitivity analysis has not been performed in our work given the large number of parameters that have to be included in it. The study remains open.

The uncertainty maps are generated by taking into account the difference between the 98th and 50th percentiles (Lombardi et al., 2005). This is built on a 95% confidence interval. By adding or removing this value from the median, the 95% confidence limit can be derived. Assuming that the GMPEs have a normal distribution, the 95% confidence interval is defined as the region between the 97.5th and 2.5th percentiles. For the two selected return periods, 475 and 975 years, the obtained results are summarized in terms of maps. Figure 11 depicts the overall uncertainty maps for PGA, SA (0.2 s), and SA (1.0 s) for B/C soil condition, with a 95% confidence interval.

The coefficient of variation, or COV, is often a better measure of the uncertainty results. It is calculated by dividing half of the 95% confidence band by the mean, which is the same as dividing the standard deviation by the mean. This quantity is used to assess the accuracy of the estimated values. The lower the COV, the more reliable the estimate is. Moreover, the coefficient of variation is an accurate parameter to appreciate the reliability of the estimated values. Following Salazar et al. (2013), the estimated COV is classified according to the criteria shown in Table 7. This range of values results from the estimated COV for PGA and SA (0.2 s). Figure 12 displays the degree of reliability for the estimated PGA and SA (0.2 s) values for the selected return periods qualitatively in terms of very high, high, medium, low, and very low degrees. It can be observed that for these two parameters, PGA and SA (0.2 s) and for both return periods, a high degree of reliability is obtained from the western part of Tipaza city toward the eastern part of Boumerdes city, including the cities of Blida and Medea. Moreover, it varies from medium to low and very low in the western part of Algiers.

As pointed out by Salazar et al. (2013), these results are very important in order to justify the use of spectral ordinates at oscillation periods of 0.2 s and 1.0 s to construct earthquake design spectra for different return periods and for given soil conditions, as done previously for the studied cities using the Malhotra approach (Malhotra, 2005). To highlight these issues, Fig. 13 displays for each studied city the

Table 9

Mean and modal seismic hazard disaggregation results (for magnitude and distance) for a return period of 475 years and 975 years, for the studied cities and for PGA

Mean and modal seismic hazard deaggregation results for PGA								
	10% in 50 years				5% in 50 years			
	PGA	$(\bar{M}, \bar{D})$	$(M^*, D^*)$	$\max H_{md}$	PGA	$(\bar{M}, \bar{D})$	$(M^*, D^*)$	$\max H_{md}$
Algiers	0.40	6.1, 8.8	5.0–5.5, 0–10	16.0%	0 PGA.55	6.2, 7.5	6.0–6.5, 0–10	16.0%
Tipaza	0.31	6.5, 16.4	7.0–7.5, 10–20	7%	0.43	6.6, 12.7	7.0–7.5, 0–20	8.6%
Boum	0.22	6.0, 13.2	5.0–5.5, 0–10	11.7%	0.31	6.1, 10.7	5.0–5.5, 0–10	12.5%
Medea	0.33	6.3, 10.5	5.0–5.5, 0–10	11.3%	0.47	6.4, 8.8	6.0–6.5, 0–10	11.3%
Blida	0.38	6.2, 9.3	5.0–5.5, 0–10	13.8%	0.53	6.3, 8.0	6.0–6.5, 0–10	13.9%

The maximum contribution for each modal scenario is displayed



seismic hazard curve with both the 95% confidence bands. The plots show the mean UHS and the mean UHS plus/minus the standard deviation, as well as the hazard curve in terms of PGA and its 95% confidence band. The obtained results give an appreciation of the uncertainty related to these parameters since they influence policy decisions on various issues, ranging from building codes to seismic risk management. Table 8 shows the PGA and its standard deviation for the two selected return periods and soil conditions at the considered cities. The supplementary material presents the results for SA (0.2 s) and SA (1.0 s).

### 8. Seismic Hazard Disaggregation Analysis

The derived seismic hazard values can be processed and exploited to define the predominant—or the most contributing—potential source of hazard and to provide the scenario design pairs of magnitude and distance throughout the so-called disaggregation process (e.g., Harmsen & Frankel, 2001). The seismic hazard disaggregation methodology was initially developed by Bernreuter (1992). Since this time, disaggregation studies have been extensively applied, discussed, and improved by many authors (e.g., Frankel, 1995; McGuire, 1995; Bazzurro & Cornell, 1999; Harmsen et al., 1999, 2000; Harmsen & Frankel, 2001; Peláez et al., 2002b; Barani et al., 2009). It is now an important tool for interpreting and understanding the contribution of various seismic sources to the seismic hazard values estimated at a specific location, as well as providing suitable solutions for earthquake design required by engineers for building purposes (McGuire, 1995).

There were some previous attempts to perform a seismic hazard disaggregation analysis on some cities in the studied area. For instance, the studies by Gherboudj et al. (2014) for Algiers and by Hamdache et al. (2019) for Blida city. In this study, the disaggregation results for the mean PGA are presented, not only in terms of magnitude and distance, but also in terms of longitude and latitude (azimuth). For the five selected cities and for the B/C soil condition. The disaggregation analysis was performed and depicted for return periods of 475 and 975 years, which is

essential in designing buildings and structures for seismic purposes. The OpenQuake Engine software (Pagani et al., 2014) was also used in the current analysis. Magnitude bins of 0.5, distance intervals of 10 km, and geographic coordinate bins of  $0.1^\circ$  were used in the computation. Figure 14 displays the obtained disaggregation results at the selected cities, for B/C soil conditions, and for return periods of 475 and 975 years, the figure depicts the contribution of each pair  $(M, D)$  to the seismic hazard, while Fig. 15 presents the disaggregation of the mean PGA results in terms of longitude and latitude. For the majority of the studied cities, the seismic hazard values for both return periods are mainly controlled by the nearest seismic foci.

Through the carried out analysis, the so-called control (Bernreuter, 1992), design (McGuire, 1995), modal (Chapman, 1995) or dominant earthquake (Bazzurro and Cornell, 1999) has been determined. In order to derive it from the contribution of the different earthquake scenarios of magnitude–distance pairs  $(M, D)$ , both the average or mean and the modal  $(M^*, D^*)$  values of the magnitude–distance pairs have been computed. The used procedure for the analysis of disaggregation results in terms of magnitude and distance is termed the 2D disaggregation technique (Bazzurro and Cornell, 1999). The following relationships, established by Bernreuter (1992), have been used in the current assessment.

$$\log \bar{D} = \frac{\sum_m \sum_d H_{md} \cdot \log d}{\sum_m \sum_d H_{md}}, \quad (17)$$

$$\bar{M} = \frac{\sum_m \sum_d H_{md} \cdot m}{\sum_m \sum_d H_{md}}, \quad (18)$$

where  $m$  is the magnitude,  $d$  is the distance, and  $H_{md}$  is the contribution to the seismic hazard of the magnitude  $m$  ( $m \pm \Delta m/2$ ) at a distance  $d$  ( $d \pm \Delta d/2$ ) for the studied site. The modal values  $(M^*, D^*)$  are the M and D values for which  $H_{md}$  is maximum. Table 9, gives the mean scenario  $(\bar{M}, \bar{D})$ , the modal scenario  $(M^*, D^*)$ , and the maximum contribution values.

### 9. Summary and Conclusions

A logic tree approach was used to conduct the seismic hazard analysis, which included two seismic models (LS and GS) and two GMPEs selected from the PEER-NGA models as well as local and regional ones. Expert judgment and an analysis of the ability of the selected GMPEs to produce accurate data were used to determine the weights of the selected GMPEs. Seismic model weights, on the other hand, were determined based on their contribution to overall seismicity. The seismic hazard maps, derived for both 10 and 5% probability of exceedance in 50 years, illustrate the results of the current assessment in terms of PGA, SA (0.2 s), and SA (1.0 s), for soil conditions B/C highlighting three main focuses within the studied region. The first one, surrounding the Mitidja Basin, dominates in terms of seismic hazard values. The remaining two foci are located in the southwest and southeast of Medea, respectively, with higher values in the southwest than in the southeast. In addition, results for five major cities in the study area were obtained for site-specific seismic hazard. The estimated PGA values at Algiers for both the selected return periods and soil condition B/C are considered consistent, according to the procedure developed by Joyner and Fumal (1985).

The UHS, on the other hand, was determined for both 475- and 975-year return times and for selected soil types. Consequently, typical SA characteristic values were derived (Table 5), which highlight the influence of the selected soil conditions. The lower PGA values are obtained for a B-type soil and for both selected return periods. Newmark–Hall type design spectra is proposed for both return periods. The computations were based on the procedure developed by Malhotra (2005), based on the SA (0.2 s) and SA (1.0 s) values. It is worthwhile to note that, unlike the current regulations in the Algerian building code (Belazougui, 2017), the proposed design spectra in this study is dependent on the soil conditions at the site under investigation.

For both return periods, 475 and 975 years, and under soil condition B/C, the overall uncertainty in the hazard calculation related to the variability in

ground-motion prediction equations is assessed and expressed in terms of 95% confidence band and coefficient of variation (COV) for estimated PGA, SA (0.2 s) and SA (1.0 s). The overall 95% confidence band is observed in the range of 0.01 to 0.60 g for a return period of 475 years, and in the range of 0.01 to 0.70 g for a 975-year return period. For both return periods, the higher values are observed around the central part of the Sahel fault (Fig. 11). As a result, the UHS results are completed by providing the standard deviation of the estimated values. Thus, the mean UHS and the standard deviation (mean UHS) are presented (Fig. 13). The resulting COV values, which represent the ground-motion variability, are used to assess the accuracy of the estimated values. The estimate is more reliable if the COV is smaller. The overall PGA and SA (0.2 s) coefficients of variation for both return periods are classified as very high, high, medium, low, and very low degrees of reliability, according to the range values in Table 7. For both return periods, Fig. 12 displays typical results. A high degree of reliability is achieved from the western part of Tipaza city to the eastern part of Boumerdes, encompassing the cities of Blida and Medea. Furthermore, close to the western part of Algiers, it ranges from medium to low and to very low (Fig. 12).

The disaggregation analysis performed provides significant results that serve as reliable tools for civil engineers and decision-makers, allowing them to develop a representative earthquake scenario during design and planning. Based on the current computations, it appears that for both the selected return periods, nearby seismicity is frequently a major contributor to the hazard at the site. Both the mean and modal values of the magnitude and distance variables were derived, and the so-called control or design earthquake is produced. The joint magnitude and distance distribution reveals a uni-modal pattern in the results obtained in the selected cities (Fig. 14). Subsequently, detailed analysis of the disaggregation of PGA values (for both 475- and 975-year return period) in azimuth (longitudes and latitudes) is carried out. Based on the current computations, the contribution of each cells is

depicted on Fig. 15 for the selected cities. The results for SA at 0.2, 1.0 and 2.0 s derived for the selected return periods and for soil condition B/C is detailed in the supplementary material. The performed analysis is carried out in accordance with the published recommendations by several authors, taking into account various U.S. regulations (e.g., U.S. Department of Energy, 1995; SSHAC, 1997; USNRC, 1997).

We believe that the results achieved not only can contribute to updating national building code provisions for earthquake-resistant construction in the investigated cities and region, but also will serve as a basis for microzoning studies in the studied cities.

#### Acknowledgements

The authors are grateful to the Editor Pr. A. Kijko, for his valuable advice. We would like to express our gratitude to the anonymous reviewers for their insightful remarks and suggestions, which considerably improved the quality of the manuscript. Research partially funded by the Programa Operativo FEDER Andalucía 2014–2020—Call made by the University of Jaén, 2018.

**Author Contributions** Conceptualization, MH; methodology, MH and JAP; validation, MH, JAP, JH and RS; formal analysis, MH and JAP; investigation, MH, JAP, JH and RS; resources, MH; data curation, MH and JAP; writing-original draft preparation, MH and JAP; writing-review and editing, MH, JAP, JH and RS; visualization, MH and JAP; supervision, MH, JAP, JH and RS; project administration, MH; funding acquisition, JAP. All authors have read and agreed to the published version of the manuscript.

#### Funding

The second author is grateful for partial financial support for this research work through the Programa Operativo FEDER Andalucía 2014–2020—Call by the University of Jaén, 2018.

#### Declarations

**Conflict of interest** The authors declare that they have no conflict of interest.

**Publisher's Note** Springer Nature remains neutral with regard to jurisdictional claims in published maps and institutional affiliations.

#### REFERENCES

- Abrahamson, N. A., Silva, W. J., & Kamai, R. (2014). Summary of the ASK14 ground motion relation for active crustal regions. *Earthquake Spectra*, 30, 1025–1055.
- Akkar, S., & Bommer, J. J. (2010). Empirical equations for the prediction of PGA, PGV, and spectral accelerations in Europe, the Mediterranean region, and the Middle East. *Seismological Research Letters*, 81(2), 195–206.
- Albarelo, D., Camassi, R., & Rebez, A. (2001). Detection of space and time heterogeneity in the completeness level of a seismic catalogue by a «robust» statistical approach: An application to the Italian area. *Bulletin of the Seismological Society of America*, 91(6), 1694–1703.
- Ambraseys, N. N., Simpson, K. U., & Bommer, J. J. (1996). Prediction of horizontal response spectra in Europe. *Earthquake Engineering & Structural Dynamics*, 25(4), 371–400.
- Atkinson, G. M., Bommer, J. J., & Abrahamson, N. A. (2014). Alternative approaches to modeling epistemic uncertainty in ground motions in probabilistic seismic-hazard analysis. *Seismological Research Letters*, 85(6), 1141–1144.
- Arroyo, D., Ordaz, M., & Rueda, R. (2014). On the selection of ground-motion prediction equations for probabilistic seismic-hazard analysis. *Bulletin of the Seismological Society of America*, 104, 1860–1875.
- Barani, S., Spallarossa, D., & Bazzurro, P. (2009). Disaggregation of probabilistic ground-motion hazard in Italy. *Bulletin of the Seismological Society of America*, 99, 2638–2661.
- Bakun, W. H. (1984). Seismic moments, local magnitudes, and coda-duration magnitudes for earthquakes in central California. *Bulletin of the Seismological Society of America*, 74, 439–458.
- Bazzurro, P., & Cornell, A. C. (1999). Disaggregation of seismic hazard. *Bulletin of the Seismological Society of America*, 89, 501–520.
- Beauval, C., Tasan, H., Laurendeau, A., Delavaud, E., Cotton, F., Guéguen, P., & Kuehn, N. (2012). On the testing of ground-motion prediction equations against small-magnitude data. *Bulletin of the Seismological Society of America*, 102(5), 1994–2007. <https://doi.org/10.1785/0120110271>
- Belabbès, S., Wicks, C., Cakir, Z., & Meghraoui, M. (2009). Rupture parameters of the 2003 Zemmouri ( $M_w$  6.8), Algeria, earthquake from joint inversion of interferometric synthetic aperture radar, coastal uplift, and GPS. *Journal of Geophysical Research*, 114, 03406. <https://doi.org/10.1029/2008JB005912>
- Belazougui, M. (2017). Algerian seismic building code: Main features of the new draft RPA 2015. 16th World Conference on

- Earthquake Engineering, 16WCEE 2017. Santiago Chile, January 9–13, 2017. Paper No. 1192
- Bender, B., and Perkins, D. M. (1987). SeisRisk III: A Computer program for seismic hazard estimation. U.S. Geological Survey Bulletin 1772. (Washington).
- Benouar, D. (1996). Seismic hazard evaluation at Algiers using Benouar's earthquake catalogue. *Natural Hazards*, 13, 119–131.
- Berneuter, D. L. (1992). Determining the control earthquake from probabilistic hazards for the proposed Appendix B. L.L.N.L. Report UCRL-JC-111964, Livermore California.
- Bommer, J. J., & Scherbaum, F. (2008). The use and misuse of logic-trees in PSHA. *Earthquake Spectra*, 24(4), 997–1009.
- Bommer, J. J., Scherbaum, F., Bungum, H., Cotton, F., Sabetta, F., & Abrahamson, N. A. (2005). On the use of logic trees for ground motion prediction equations in seismic hazard assessment. *Bulletin of the Seismological Society of America*, 95(2), 377–389.
- Bommer, J. J., & Abrahamson, N. A. (2006). Why do modern probabilistic seismic-hazard analyses often lead to increased hazard estimates? *Bulletin of the Seismological Society of America*, 96(6), 1967–1977.
- Bommer, J. J., Stafford, P. J., Alarcon, J. E., & Akkar, S. (2007). The influence of magnitude range on empirical ground-motion prediction. *Bulletin of the Seismological Society of America*, 97(6), 2152–2170.
- Bommer, J. J., Douglas, J., Scherbaum, F., Cotton, F., Bungum, H., & Fäh, D. (2010). On the selection of ground-motion prediction equations for seismic hazard analysis. *Seismological Research Letters*, 81(5), 783.
- Bommer, J. J., & Montaldo Falero, V. (2020). Virtual fault ruptures in area-source zones for PSHA: Are they always needed? *Seismological Research Letters*. <https://doi.org/10.1785/0220190345>
- Boore, D. M., & Atkinson, G. M. (2008). Ground-motion prediction equations for the average horizontal component of PGA, PGV, and 5%-damped PSA at spectral periods between 0.01 s and 10.0 s. *Earthquake Spectra*, 24, 99–138.
- Boore, D. M., Stewart, J. P., Seyhan, E., Gail, M., & Atkinson, G. A. (2014). NGA-West2 equations for predicting PGA, PGV, and 5% damped PSA for shallow crustal earthquakes. *Earthquake Spectra*, 30, 1057–1085.
- Bozzoni, F., Corigliano, M., Lai, C. G., Salazar, W., Scandella, L., Zuccolo, E., Latchman, J., Lynch, L., & Robertson, R. (2011). Probabilistic seismic hazard assessment at the eastern Caribbean Islands. *Bulletin of the Seismological Society of America*, 101(5), 2499–2521. <https://doi.org/10.1785/0120100208>
- BSSC-Building Seismic Safety Council. (2003). *NEHRP recommended provisions for seismic regulations for new buildings and other structures, part1: provisions, FEMA 368*. Federal Emergency Management Agency.
- Cetin, E., Meghraoui, M., Cakir, Z., Akoglu, A. M., Mimouni, O., & Chebbah, M. (2012). Seven years of postseismic deformation following the 2003 Mw = 6.8 Zemmouri earthquake (Algeria) from InSAR time series. *Geophysical Research Letters*, 39, 10307. <https://doi.org/10.1029/2012GL051344>, 2012
- Chapman, M. C. (1995). A probabilistic approach to selection of ground motions for engineering design. *Bulletin of the Seismological Society of America*, 85, 937–942.
- Campbell, K. W., & Bozorgnia, Y. (2008). NGA ground motion model for the geometric mean horizontal component of PGA, PGV, PGD and 5% damped linear-elastic response spectra for periods ranging from 0.01 and 10.0 s. *Earthquake Spectra*, 24, 139–171.
- Campbell, K. W., & Bozorgnia, Y. (2014). NGA-West2 ground motion model for the average horizontal components of PGA, PGV, and 5%-damped linear acceleration response spectra. *Earthquake Spectra*, 30, 1087–1115.
- Campbell, K. W., & Gupta, N. (2018). Modeling diffuse seismicity in probabilistic seismic hazard analysis: treatment of virtual faults. *Earthquake Spectra*, 34(3), 1135–1154.
- Cauzzi, C., Faccioli, E., Vanini, M., & Bianchini, A. (2015). Updated predictive equations for broadband (001–10 s) horizontal response spectra and peak ground motions, based on a global dataset of digital acceleration records. *Bulletin of Earthquake Engineering*, 13(6), 1587–1612.
- Chiou, B. S. J., & Youngs, R. R. (2008). An NGA model for the average horizontal component of peak ground motion and response spectra. *Earthquake Spectra*, 24, 173–215.
- Chiou, B. S. J., & Youngs, R. R. (2014). Update of the Chiou and Youngs NGA model for the average horizontal component of peak ground motion and response spectra. *Earthquake Spectra*, 30(3), 1117–1153.
- Cooke, P. (1979). Statistical inference for bounds of random variables. *Biometrika*, 66, 367–374.
- Cornell, C. A. (1968). Engineering seismic risk analysis. *Bulletin of the Seismological Society of America*, 58(1), 1583–1606.
- Cotton, F., Scherbaum, F., Bommer, J. J., & Bungum, H. (2006). Criteria for selecting and adjusting ground-motion models for specific target applications: Applications to Central Europe and rock sites. *Journal of Seismology*, 10(2), 137–156.
- Cramer, C. H. (2001). A seismic hazard uncertainty analysis for the New Madrid seismic zone. *Engineering Geology*, 62, 251–266.
- Cramer, C. H., Petersen, M. D., & Reichel, M. S. (1996). A Monte Carlo approach in estimating uncertainty for a seismic hazard assessment of Los Angeles, Ventura and Orange Counties, California. *Bulletin of the Seismological Society of America*, 86(6), 1681–1691.
- Cramer, C. H., Wheeler, R. L., & Mueller, C. S. (2002). Uncertainty analysis for seismic hazard in the Southern Illinois Basin. *Seismological Research Letters*, 73(5), 792–805.
- Crowley, H., Monelli, D., Pagani, M., Silva, V., Weatherill, G. (2011). OpenQuake book. The GEM Foundation, Pavia, Italy.
- Delavaud, E., Scherbaum, F., Kühn, N., & Riggelsen, C. (2009). Information-theoretic selection of ground-motion prediction equations for seismic hazard analysis: An applicability study using Californian data. *Bulletin of the Seismological Society of America*, 99(6), 3248–3263.
- Delavaud, E., Cotton, F., Beauval, C., Akkar, S., Scherbaum, F., and Danciu, L. (2012a). Construction of a ground-motion logic tree for PSHA in Europe within the SHARE project. 15 WCEE, Lisboa, Portugal
- Delavaud, E., Cotton, F., Akkar, S., Scherbaum, F., Danciu, L., Beauval, C., Drouet, S., Douglas, J., Basili, R., Sandikkaya, M. A., Segou, M., Faccioli, E., & Theodoulidis, N. (2012b). Toward a ground-motion logic tree for probabilistic seismic hazard assessment in Europe. *Journal of Seismology*, 16, 451–473. <https://doi.org/10.1007/s10950-012-9281-z>
- Delavaud, E., Scherbaum, F., Kühn, N., & Allen, T. (2012c). Testing the global applicability of ground-motion prediction equations for active shallow crustal regions. *Bulletin of the Seismological Society of America*, 102(2), 707–721. <https://doi.org/10.1785/0120110113>

- Delvaux, D., & Sperner, B. (2003). New aspects of tectonic stress inversion with reference to the TENSOR program. *Geological Society, London, Special Publications.*, 212, 75–100.
- Delouis, B., Vallee, M., Meghraoui, M., Calais, E., Maouche, S., Lammali, K., Mahras, A., Briole, P., Benhamouda, F., & Yelles, K. (2004). Slip distribution of the 2003 Boumerdes Zemmouri earthquake, Algeria, from teleseismic, GPS, and coastal uplift data. *Geophysical Research Letters*, 31, L18607. <https://doi.org/10.1029/2004GL020687>
- Déverchère, J., Yelles, K., Domzig, A., Mercier de Lépinay, B., Bouillin, J. P., Gaullier, V., Bracène, R., Calais, E., Savoye, B., Kherroubi, A., Le Roy, P., Pauc, H., & Dan, G. (2005). Active thrust faulting offshore Boumerdes Algeria, and its relations to the 2003 Mw 6.9 earthquake. *Geophysical Research Letters*, 32, 04311. <https://doi.org/10.1029/2004GL021646>
- Douglas, J. (2003). Earthquake ground motion estimation using strong motion records: A review of equations for the estimation of peak ground acceleration and response spectral ordinates. *Earth-Science Reviews*, 61(1/2), 43–104.
- Douglas, J. (2007). On the regional dependence of earthquake response spectra. *ISET Journal of Earthquake Technology*, 44(1), 71–99.
- Eurocode 8 (2004) Design of structures for earthquake resistance—Part 1: general rules, seismic actions and rules for buildings. EN 1998–1: 2004. Comité Européen de Normalisation, Brussels
- EPRI-Electric Power Research Institute, 1986. Seismic hazard methodology for the central and eastern United States. EPRI Report NP-4726, Palo Alto, CA.
- Faccioli, E., Bianchini, A., and Villani, M. (2010). New ground motion prediction equations for  $T > 1$  s and their influence on seismic hazard assessment. Proceedings of the University of Tokyo Symposium on Long-Period Ground Motion and Urban Disaster Mitigation, March 17–18, 2010
- Field, E. H., Jackson, D. D., & Dolan, J. F. (1999). A mutually consistent seismic-hazard source model for Southern California. *Bulletin of the Seismological Society of America*, 89(3), 559–578.
- Field, E. H., Jordan, T. H., & Cornell, C. A. (2003). OpenSHA—A developing community-modeling environment to seismic hazard analysis. *Seismological Research Letters*, 74, 406–419.
- Frankel, A. (1995). Mapping seismic hazard in the central and eastern United States. *Seism. Res. Lett.*, 66, 8–21.
- Frankel, A., Muller, C. S., Barnhard, T. P., Leyendecker, E. V., Wesson, R. L., Harmsen, S. C., Klein, F. W., Perkins, D. M., Dickman, N. C., Hanson, S., & Hopper, M. G. (2000). USGS national seismic hazard maps. *Earthquake Spectra*, 16, 1–19.
- Gardner, J. K., & Knopoff, L. (1974). Is the sequence of earthquakes in Southern California, with aftershocks removed, Poissonian? *Bulletin of the Seismological Society of America*, 64, 1363–1367.
- Gherboudj, F., & Laouami, N. (2014). Scalar and vector probabilistic seismic hazard analysis: Application for Algiers City. *Journal of Seismology*, 18, 319–330. <https://doi.org/10.1007/s10950-013-9380-5>
- Gutenberg, B., & Richter, C. F. (1944). Frequency of earthquakes in California. *Bulletin of the Seismological Society of America*, 34, 185–188.
- Hamdache, M., Peláez, J. A., Talbi, A., & López Casado, C. (2010). A unified catalog of main earthquakes for Northern Algeria from A.D. 856 to 2008. *Seis. Res. Lett.*, 81, 732–739.
- Hamdache, M., Peláez, J. A., Talbi, A., Mobarki, M., & López Casado, C. (2012). Ground-motion hazard values for Northern Algeria. *Pure and Applied Geophysics*, 169, 711–723.
- Hamdache, M., Peláez, J.A., Yelles-Chaouche, A., Monteiro, R., Marques, M., Castro, M., Beldjoudi, H., and Kherroubi, A. (2019). A Preliminary Seismic Hazard Modelling in Northern Algeria. Springer Nature Switzerland AG 2019. N. Sundararajan et al. (eds.), On Significant Applications of Geophysical Methods, Advances in Science, Technology & Innovation, [https://doi.org/10.1007/978-3-030-01656-2\\_53](https://doi.org/10.1007/978-3-030-01656-2_53).
- Harbi, A., Maouche, S., Vaccari, F., Aoudia, A., Oussadou, F., Panza, G. F., & Benouar, D. (2007). Seismicity, seismic input and site effects in the Sahel Algiers region (North Algeria). *Soil Dynamics and Earthquake Engineering*, 27(5), 427–447.
- Harbi, A., Sebaï, A., Benmedjber, M., Ousadou, F., Rouchiche, Y., Grigahcene, A., Aïni, D., Bourouis, S., Maouche, S., & Ayadi, A. (2015). The Algerian Homogenized Macroseismic Database (267–1989): A deeper Insight into the Algerian Historical Seismicity. *Seismological Research Letters*, 86(6), 1705–1716.
- Harmsen, S., & Frankel, A. (2001). Geographic deaggregation of seismic hazard in the United States. *Bulletin of the Seismological Society of America*, 91, 13–26.
- Harmsen, S., Perkins, D., & Frankel, A. (1999). Deaggregation of probabilistic ground motions in the Central and Eastern United States. *Bulletin of the Seismological Society of America*, 89, 1–13.
- Harmsen, S., Klein, W., Perkins, D. M., Dickman, N. C., Hanson, S., & Hopper, M. G. (2000). USGS national seismic hazard maps. *Earthquake Spectra*, 16, 1–19.
- Heddar, A., Authemayou, C., Djellit, H., Yelles, A. K., Déverchère, J., Gharbi, S., Boudiaf, A., & Van Vliet Lanoe, B. (2013). Preliminary results of a paleoseismological analysis along the Sahel fault (Algeria): New evidence for historical seismic events. *Quaternary International*, 302, 210–223.
- Heaton, T. H., Tajima, F., & Mori, A. W. (1986). Estimating ground motions using recorded accelerograms. *Surveys in Geophysics*, 8, 25–83.
- IASPEI (International Association of Seismology and Physics of the Earth's Interior) (2005) Summary of Magnitude Working Group recommendations on standard procedures for determining earthquake magnitudes from digital data, available at: [ftp://ftp.iaspei.org/pub/commissions/CSOI/summary\\_of\\_WG\\_recommendations\\_2005.pdf](ftp://ftp.iaspei.org/pub/commissions/CSOI/summary_of_WG_recommendations_2005.pdf)
- ICC. (2009). *International building code 2009*. International Code Council.
- Idriss, I. M. (2014). An NGA-West2 empirical model for estimating the horizontal spectral values generated by shallow crustal earthquakes. *Earthquake Spectra*, 30, 1155–1177.
- Johnston, A. C. (1996). Seismic moment assessment of earthquakes in stable continental regions I. Instrumental Seismicity. *Geophysical Journal International*, 124, 381–414.
- Joyner, W. B., and Fumal, T. E. (1985). Predictive mapping of earthquake ground motion, In: J. I. Zione (ed.), Evaluating Earthquake Hazards in the Los Angeles Region – An Earth Science Perspective, USGS Professional Paper 1360, Washington D.C.
- Kale, O., & Akkar, S. (2017). A ground-motion logic-tree scheme for regional seismic hazard studies. *Earthquake Spectra*, 33, 837–856.
- Kanamori, H. (1977). The energy release in great earthquakes. *Journal of Geophysical Research*, 82, 2981–2987.



- Kanamori, H. (1983). Magnitude scale and quantification of earthquakes. *Tectonophysics*, 93(3–4), 185–199.
- Kagan, Y. (2002). Seismic moment distribution revisited: I. Statistical results. *Geophysical Journal International*, 148(3), 520–541.
- Kijko, A. (2004). Estimation of the maximum magnitude,  $m_{max}$ . *Pure and Applied Geophysics*, 161, 1655–1681.
- Kijko, A., & Singh, M. (2011). Statistical tools for the maximum possible earthquake magnitude estimation. *Acta Geophys*, 5, 674–700.
- Kijko, A., Smit, A., & Sellevoll, M. A. (2016). Estimation of earthquake hazard parameters from incomplete data files. Part III. Incorporation of uncertainty of earthquake-occurrence model. *Bulletin of the Seismological Society of America*, 106, 1210–1222.
- Kulkarni, R. B., Youngs, R. R., and Coppersmith, K. J. (1984). Assessment of confidence intervals for results of seismic hazard analysis. In Proceedings of the Eighth World Conference on Earthquake Engineering, San Francisco, vol. 1, 263–270. Englewood Cliffs, NJ: Prentice Hall.
- Laouami, N., Slimani, A., & Larbes, S. (2018). Ground motion prediction equations for Algeria and surrounding region using site classification based H/V spectral ratio. *Bulletin of Earthquake Engineering*. <https://doi.org/10.1007/s10518-018-0310-3>
- Lapajne, J. K., Sket Motnikar, B., Zabukovec, B., & Zupancic, P. (2003). Probabilistic seismic hazard assessment methodology for distributed seismicity. *Bulletin of the Seismological Society of America*, 93, 2502–2515.
- Linkimer, L. (2008). Relationship between peak ground acceleration and modified Mercalli intensity in Costa Rica. – *Revista Geol. De Amér. Central*, 38, 81–94.
- Lombardi, A. M., Akinci, A., Malagnini, L., and Mueller, C. S. (2005). Uncertainty analysis for seismic hazard in Northern and Central Italy. *Annals of Geophysics*, 48(6), 853–865.
- López Casado, C., Molina, S., Delgado, J., & Peláez, J. A. (2000). Attenuation of intensity with epicentral distance in the Iberian Peninsula. *Bulletin of the Seismological Society of America*, 90, 34–47.
- Maouche, S., Meghraoui, M., Morhange, C., Belabbes, S., Bouhadad, Y., & Haddoum, H. (2011). Active coastal thrusting and folding, and uplift rate of the Sahel Anticline and Zemmouri earthquake area (Tell Atlas, Algeria). *Tectonophysics*, 509(2011), 69–80. <https://doi.org/10.1016/j.tecto.2011.06.003>
- Maiti, S. K., Nath, S. K., Adhikari, M. D., Srivastara, N., Sengupta, P., & Gupta, A. K. (2017). Probabilistic seismic hazard model of west Bengal. *Journal of Earthquake Engineering*, 21(7), 113–1157. <https://doi.org/10.1080/13632469.2016.1210054>
- Malhotra, P. K. (2005). Return period of design ground motions. *Seismological Research Letters*, 76, 693–699.
- Mandal, H. S., Shukla, A. K., Khan, K., & Mishra, O. P. (2013). A new insight into Probabilistic seismic hazard analysis for Central India. *Pure and Applied Geophysics*. <https://doi.org/10.1007/s00024-013-0666-x>
- Matthews, M. V., Ellsworth, W. L., & Reasenber, P. A. (2002). A Brownian model for recurrent earthquakes. *Bulletin of the Seismological Society of America*, 92, 2233–2250.
- Mak, S., Clements, R. A., & Schorlemmer, D. (2017). Empirical evaluation of hierarchical ground-motion models: Score uncertainty and model weighting. *Bulletin of the Seismological Society of America*, 107, 949–965.
- McGuire, R. K. (1977). Effects of uncertainty in seismicity on estimates of seismic hazard for the east coast of the United States. *Bulletin of the Seismological Society of America*, 67, 827–848.
- McGuire, R. K. (1995). Probabilistic seismic hazard analysis and design earthquakes: Closing the loop. *Bulletin of the Seismological Society of America*, 85, 1275–1284.
- McGuire, R. K. (2004). Seismic Hazard and Risk Analysis, EERI Monograph MNO-10, Earthquake Engineering Research Institute, El Cerrito, CA, 187 pp.
- McGuire, R. K., & Shedlock, K. M. (1981). Statistical Uncertainty in seismic hazard evaluations in the United States. *Bulletin of the Seismological Society of America*, 71, 1287–1308.
- Meghraoui, M. (1991). Blind reverse faulting system associated with the Mont ChenouaTipasa earthquake of 29 October 1989 (north-central Algeria). *Terra Nova*, 3, 84–93.
- Meghraoui, M., & Doumaz, F. (1996). Earthquake-induced flooding and paleoseismicity of the El Asnam (Algeria) fault related fold. *Journal of Geophysical Research*, 101, 17617–17644.
- Mezcua J (2002) Seismic engineering course (in Spanish). Universidad Politécnica de Madrid
- Mignan, A., and Woessner, J. (2012). Estimating the magnitude of completeness in earthquake catalogs, Community Online Resource for Statistical Seismicity Analysis, doi:<https://doi.org/10.5078/corssa-00180805>. Available at <http://www.corssa.org>
- Monelli, D., Pagani, M., Weatherill, G., Danciu, L., & Garcia, J. (2014). Modeling distributed seismicity for probabilistic seismic-hazard analysis: Implementation and insights with the Open-Quake engine. *Bulletin of the Seismological Society of America*, 104(4), 1636–1649. <https://doi.org/10.1785/0120130309>
- Morel, J. L., & Meghraoui, M. (1996). The Goringe Alboran-Tell (Galtel) tectonic zone: A transpression system along the Africa-Eurasia plate boundary. *Geology*, 24, 755–758.
- Murphy, J. R., & O'Brien, L. J. (1977). The correlation of peak ground acceleration amplitude with seismic intensity and other physical parameters. *Bulletin of the Seismological Society of America*, 67, 877–915.
- Newmark, N. M., and Hall, W. J. (1982). Earthquake spectra and design. Earthquake Engineering Research Institute Monograph Series no. 3, Berkeley, California, USA.
- Pace, B., Visini, F., & Peruzza, L. (2016). FiSH: MATLAB tools to turn fault data into seismic-hazard models. *Seismological Research Letters*, 87(2A), 374–386.
- Pagani, M., Monelli, D., Weatherill, G., Danciu, L., Crowley, H., Silva, V., Henshaw, P., Butler, L., Nastasi, M., Panzeri, L., Simionato, M., & Vigano, D. (2014). OpenQuake-engine: An open hazard (and risk) software for the global earthquake model. *Seismological Research Letters*, 85, 692–702. <https://doi.org/10.1785/0220130087>
- Patel, J. K., Kapadia, C. H., & Owen, D. B. (1976). *Handbook of statistical distributions*. Marcel Dekker.
- Peláez, J. A., & López Casado, C. (2002). Seismic hazard estimate at the Iberian Peninsula. *Pure and Applied Geophysics*, 59, 2699–3273.
- Peláez, J. A., López Casado, C., & Henares, J. (2002). Deaggregation in magnitude, distance and azimuth in the south and west of the Iberian Peninsula. *Bulletin of the Seismological Society of America*, 92, 2177–2185.
- Peláez, J. A., Hamdache, M., & Lopez Casado, C. (2003). Seismic hazard in Northern Algeria using spatially-smoothed seismicity.



- Results for Peak Ground Acceleration, Tectonophys.*, 372, 105–119.
- Peláez, J. A., Hamdache, M., & Lopez Casado, C. (2005a). Updating the probabilistic seismic hazard values of Northern Algeria with the 21 May 2003 M 6.8 Algiers earthquake included. *Pure and Applied Geophysics*, 162, 2163–2177.
- Peláez, J. A., Delgado, J., & Lopez Casado, C. (2005b). A preliminary probabilistic seismic hazard in terms of Arias intensity in southeastern Spain. *Engineering Geology*, 77, 139–151. <https://doi.org/10.1016/j.enggeo.2004.09.002>
- Peláez, J. A., Hamdache, M., & Lopez Casado, C. (2006a). Seismic hazard in terms of spectral accelerations and uniform hazard spectra in Northern Algeria. *Pure and Applied Geophysics*, 163, 119–135.
- Peláez, J. A., Hamdache, M., Lopez Casado, C. (2006b) Strong ground motion in the 21 May 2003 Algiers, Algeria, earthquake. 5<sup>th</sup> Hispano–Portugues Assembly of Geodesy and Geophysics, Sevilla, Spain.
- Peláez, J. A., Hamdache, M., Sanz de Galdeano, C., Sawires, R., and García Hernández, M. T. (2016). Forecasting moderate earthquakes in Northern Algeria and Morocco in Earthquake and their impact on society (S. D'Amico, ed.), Springer, Natural Hazards, 81–95.
- Peláez, J. A., Henares, J., Hamdache, M., and Sanz de Galdeano, C (2018a) A seismogenic zone model for seismic hazard studies in Northwestern Africa in Moment tensor solutions. A useful tool for seismotectonics (S. D'Amico, ed.), Springer Natural Hazards, 643–680.
- Peláez, J. A., Henares, J., Hamdache, M., and Sanz de Galdeano, C. (2018b). An updated seismic model for the northwestern Africa. 16 E.C.E. Eng. Thessaloniki, 18–21 June 2018b
- Peruzza, L., & Pace, B. (2002). Sensitivity analysis for seismic source characteristics to probabilistic seismic hazard assessment in central Apennines (Abruzzo area). *Bollettino Di Geofisica Teorica Ed Applicata*, 43, 79–100.
- Peruzza, L., Pace, B., & Cavallini, F. (2010). Error propagation in time-dependent probability of occurrence for characteristic earthquakes in Italy. *J. Sei.*, 14(1), 119–141. <https://doi.org/10.1007/s10950-008-9131-1>
- Petersen, M. D., Moschetti, M. P., Powers, P. M., Mueller, C. S., Haller, K. M., Frankel, A. D., Zeng, Y., Rezaeian, S., Harmsen, S. C., Boyd, O. S., Field, N., Chen, R., Rukstales, K. S., Luco, N., Wheeler, R. L., Williams, R.A., and Olsen, A. H. (2015) The 2014 United States National Seismic Hazard Model: Earthquake Spectra 31(1):1–30. <https://doi.org/10.1193/120814EQS210M>.
- RPA99. (2003). Règlement Parasismique Algérien. CGS Earthquake Engineering Research Center, Rue Kaddour Rahim, BP 252, Hussein Dey, Algiers, Algeria
- Roselli, P., Marzocchi, W., & Faenza, F. (2016). Toward a new probabilistic framework to score and merge ground motion prediction equations: The case of the Italian region. *Bulletin of the Seismological Society of America*, 106(2), 720–733. <https://doi.org/10.1785/0120150057>
- Rueda, J., & Mezcuá, J. (2002). Study of the 23 September 2003, Pego (Alicante) earthquake. Obtaining a *mbLg-MW* relationship for the Iberian Peninsula. *Revista De La Sociedad Geológica De España*, 15, 159–173. (In Spanish).
- Salazar, W., Brown, L., & Mannette, G. (2013). Probabilistic seismic hazard assessment for Jamaica. *Journal of Civil Engineering and Architecture*, 7(9), 1118–1140. ISSN 1934-7359.
- Scherbaum, F., Delavaud, E., & Riggelsen, C. (2009). Model selection in seismic hazard analysis: An information-theoretic perspective. *Bulletin of the Seismological Society of America*, 99(6), 3234–3247.
- Shumway, A. M., Petersen, M. D., Powers, P. M., and Rezaeian, S. (2018). Additional period and site class maps for the 2014 National Seismic Hazard Model for the conterminous United States: US. G.S. Open-File Report 2018–1111, 46 p., <https://doi.org/10.3133/ofr20181111>.
- Secanell, R., Martin, C., Viallet, E., & Senfaute, G. (2018). A Bayesian methodology to update the probabilistic seismic hazard assessment. *Bulletin of Earthquake Engineering*, 16, 2513–2527.
- Senior Seismic Hazard Analysis Committee (SSHAC) (1997) Recommendations for probabilistic seismic hazard analysis: guidance on uncertainty and use of experts, Lawrence Livermore National Laboratory. Report UCRL-ID-122160, U.S. Nuclear Regulatory Commission Report NUREG/CR-6372.
- Sparacino, F., Palano, M., Peláez, J. A., & Fernández, J. (2020). Geodetic deformation versus seismic crustal moment-rate: Insights from the Ibero-Maghrebian region. *Remote Sensing*. <https://doi.org/10.3390/rs12060952>
- Stafford, P. J., Strasser, F. O., & Bommer, J. J. (2008). An evaluation of the applicability of the NGA models to ground-motion prediction in the Euro-Mediterranean region. *Bulletin of Earthquake Engineering*, 6(2), 149–177.
- Stepp, J. C. (1972). Analysis of completeness of the earthquake sample in the Puget Sound area and its effect on statistical estimates of earthquake hazard. In: Proceedings First Microzonation Conference, Seattle, U.S.A., 897–909
- Stewart, J. P., Douglas, J., Javanbarg, M., Bozorgnia, Y., Abrahamson, N. A., Boore, D. M., & Stafford, P. J. (2015). Selection of ground motion prediction equations for the Global Earthquake Model. *Earthquake Spectra*, 31(1), 19–45.
- Thenhaus, P. C., and Campbell, K. W. (2003). Seismic hazard analysis, in Earthquake Engineering Handbook (W.-F. Chen and C. Scawthorn, eds.), Chapter 8, CRC Press, 50 pp
- Tinti, S., & Mulargia, F. (1985). Completeness analysis of a seismic catalog. *Annales Geophysicae*, 3, 407–414.
- U.S. Department of Energy (1995) Natural phenomena hazards assessment criteria, U.S. Department of Energy Standard Report DOE-STD-1023–95.
- U.S. Nuclear Regulatory Commission (USNRC) (1997) Identification and characterization of seismic sources and determination of safe shutdown earthquake ground motion. Appendix C: Determination of controlling earthquakes and development of seismic hazard information base, in Regulatory Guide 1.165, Office of Nuclear Regulatory Research, Washington, D.C.
- Visini, F., Valentini, A., Chartier, T., Scotti, O., & Pace, B. (2020). Computational tools for relaxing the fault segmentation in probabilistic seismic hazard modeling in complex fault system. *Pure and Applied Geophysics*, 177, 1855–1877. <https://doi.org/10.1007/s00024-019-02114-6>
- Weichert, D. H. (1980). Estimation of the earthquake recurrence parameters for unequal observation periods for different magnitudes. *Bulletin of the Seismological Society of America*, 70(4), 1337–1346.
- Wells, D. L., & Coppersmith, K. L. (1994). New empirical relationship among magnitude, rupture length, rupture width, rupture area, and surface displacement. *Bulletin of the Seismological Society of America*, 84, 74–1002.

- Wen, Y. K. (2004). Probabilistic aspects of earthquake engineering in Earthquake engineering. From engineering seismology to performance-based engineering (Bozorgnia, Y., and Bertero, V.V., eds.), CRC Press, Boca Raton, Florida
- Xu, W. (2019). Probabilistic seismic hazard assessment using spatially smoothed seismicity in North China seismic zone. *Journal of Seismology*, 23, 613–622. <https://doi.org/10.1007/s10950-019-09825-2>
- Yazdani, A., Shahidzadeh, M. S., & Takada, T. (2021). Merging data and experts' knowledge-based weights for ranking GMPEs. *Earthquake Spectra*, 37(2), 857–875. <https://doi.org/10.1177/8755293020970974>
- Yelles-Chaouche, A. K., Djellit, H., Haned, S., Deramchi, A., Allili, T., Kherroubi, A., Beldjoudi, H., Semmane, F., Amrani, A., Haddana, Z., Chaoui, F., Aidi, A., & Allili, A. (2007). The Algerian digital network. *European-Mediterranean Seismological Centre Newsletter*, 22, 7–8.
- Yelles-Chaouche, A. K., Domzig, A., Déverchère, J., Bracène, R., Mercier de Lépinay, B., Strzeczynski, P., Bertrand, G., Boudiaf, A., Winter, T., Kherroubi, A., Le Roy, P., & Djellit, H. (2009). Plio-quaternary reactivation of the Neogene margin off NW Algiers, Algeria: The Khayr-Al-Din bank. *Tectonophysics*, 475, 98–116.

(Received December 4, 2021, revised February 26, 2022, accepted May 12, 2022, Published online June 9, 2022)